Journal of Materials Chemistry B

Accepted Manuscript

This article can be cited before page numbers have been issued, to do this please use: J. Zhao, L. Huang, X. Cui, S. Li and H. Wu, *J. Mater. Chem. B*, 2015, DOI: 10.1039/C5TB01857A.

ROYAL SOCIETY OF CHEMISTRY

www.rsc.org/materialsB

View Article Online
DOI: 10.1039/C5TB01857A
PAPER

Cite this: DOI: 10.1039/c0xx00000x

www.rsc.org/xxxxxx

Maximizing the Thiol-Activated Photodynamic and Fluorescence Imaging Functionalities of Theranostic Reagents by Modularization of the Bodipy-based Dyad Triplet Photosensitizers

Jianzhang Zhao,[a]* Ling Huang,[a] Xiaoneng Cui,[a] Shujing Li,[b] and Huijian Wu[b]*

Received (in XXX, XXX) Xth XXXXXXXXX 20XX, Accepted Xth XXXXXXXXX 20XX
DOI: 10.1039/b000000x

To maximize both the activatable singlet oxygen ($^1O_2$) production and fluorescence of theranostic photodynamic (PDT) reagents, herein we propose a modularized molecular structural profile, i.e. the intersystem crossing (ISC) and the fluorescence functionalities were accomplished with *different* modules in a dyad, thus the activated $^1O_2$ production yield (Φ_Δ, PDT) and the fluorescence yield (Φ_F) can *both* approach 100%. The PDT and the fluorescence were caged with thiol-cleavable disulfide bond (−S−S−) linker and electron trap (2,4-dinitrobenzenesulfide, DNBS). This new molecular structural profile is different from the conventional theranostic PDT reagents, which are based on single chromophore for both PDT and fluorescence, thus the limitation of $\Phi_\Delta + \Phi_F = 100\%$ exists, only half of our new molecular profile. To this end six Bodipy dyads were prepared. The photophysical properties of the dyads were studied with steady state absorption/fluorescence spectroscopies and nanosecond transient absorption spectroscopy. The dyads show weak PDT and luminescence, due to the caging effect. In the presence of thiols (GSH or Cys), cleavage of disulfide linker and DNBS occurred, the PDT and fluorescence modules were activated simultaneously (Φ_F: 1.3%→47.6%; Φ_Δ: 16.7%→71.5%). These results are useful for designing of activatable PDT/fluorescence imaging theranostic reagents.

Introduction

Photodynamic therapy (PDT) reagents are in particular interest due to its ability of production of cytotoxic singlet oxygen ($^1O_2$) upon photoiiradiation.[1–6] Among the other desired properties, strong absorption of visible or near-IR light, high triplet excited state yield, low dark toxicity are crucial for PDT reagents. Porphyrin derivatives were used as the first generation PDT reagents.[3] Recently, activatable PDT reagents were developed, such as acid-activatable iodo-azaBodipy derivatives,[4,7–10] porphyrin compounds,[11–13] PDT molecular beacons,[14–16] or photoswitched $^1O_2$ production with photochromic chromophores.[17] However, switching of the triplet excited states of organic chromophores was not studied in detail with nanosecond time-resolved transient absorption spectroscopy.[18] In-depth investigation into the variation of the triplet excited state with time-resolved spectroscopy will be useful for future design of the activatable PDT reagents.

Moreover, it is highly desired to develop PDT reagents which give activated $^1O_2$ photosensitizing *and* luminescence at the same time, so that treatment/monitoring bifunctional theranostic reagents can be attained.[19] However, investigations on these PDT compounds are rare.[19] Actually there is a dilemma for these bifunctional PDT compounds since these reagents are usually based on a *single* chromophore profile, as a result, the efficient ISC required for producing of triplet excited state will inevitably quench the fluorescence of the same chromophore, and the maximal sum of the yield of the two competing processes of ISC and fluorescence will be less than 100%. In order to address this challenge and to maximize the luminescence efficiency, *as well as* the PDT effect, the two functionalities can be accomplished by *separate* chromophores, for example in a dyad, which are able to be simultaneously activated by cancer-related biomarkers, such as high concentration of biological thiols (GSH and Cys).

PDT reagents based on fluorescence-resonance-energy-transfer (FRET) mechanism have been reported, e.g. photodynamic molecular beacon,[16] or the photosensitizer aptamer switch.[20] In these activatable PDT reagents, usually a photosensitizer and a quencher, such as black hole quencher, was linked by cleavable bonds or aptamers. Targeted cleavage of the linker or binding to specific enzyme or biomarkers for disease (small molecules) will activate the PDT reagents. Porphyrin and Rhodamine was used to construct a caspase-specific luminescent imaging reagents with the ability of induce cell death and at the same time, to monitor the cell death by ratiometric fluorescence.[12] However, in that case the PDT effect was not caged. Recently phthalocyanine complex was caged with 2,4-dinitrobenzenesulfide, the phthalocyanine chromophore acts as PDT as well as the fluorescence module.[19a]

In this case the single chromophore play both the fluorescence and triplet state production roles. A Bodipy dyad was reported to show thiol activatable fluorescence, but the PDT effect was not caged.[19b]

In order to address the above challenges, herein we prepared Bodipy-iodoBodipy dyads (Scheme 1) to achieve the following goals: (a) to attain *simultaneous* thiol-activated fluorescence and PDT effect with *different* chromophores in a dyad, for which the PDT and the fluorescence was caged; (b) feasibly tuneable fluorescence emission wavelength, which offer the feasibility for multi-colour luminescent imaging; (c) the switching of the triplet excited state is thoroughly studied with the nanosecond transient absorption spectroscopy. The activated PDT and the fluorescence was achieved with separate modules in a caged dyad, thus either the $^1O_2$ production or the fluorescence can be maximized, which is different from the conventional theranostic PDT materials which contain a single chromophore.[19a] The caging of the PDT property and the fluorescence was achieved with different approaches, such as FRET and electron transfer. Thiol-cleavable disulfide bond (−S−S−) was used as the linker between the PDT and the fluorescence modules.[21–27] These results are useful for future designing of activatable theranostic PDT reagents and for real-time treatment/monitoring.[12]

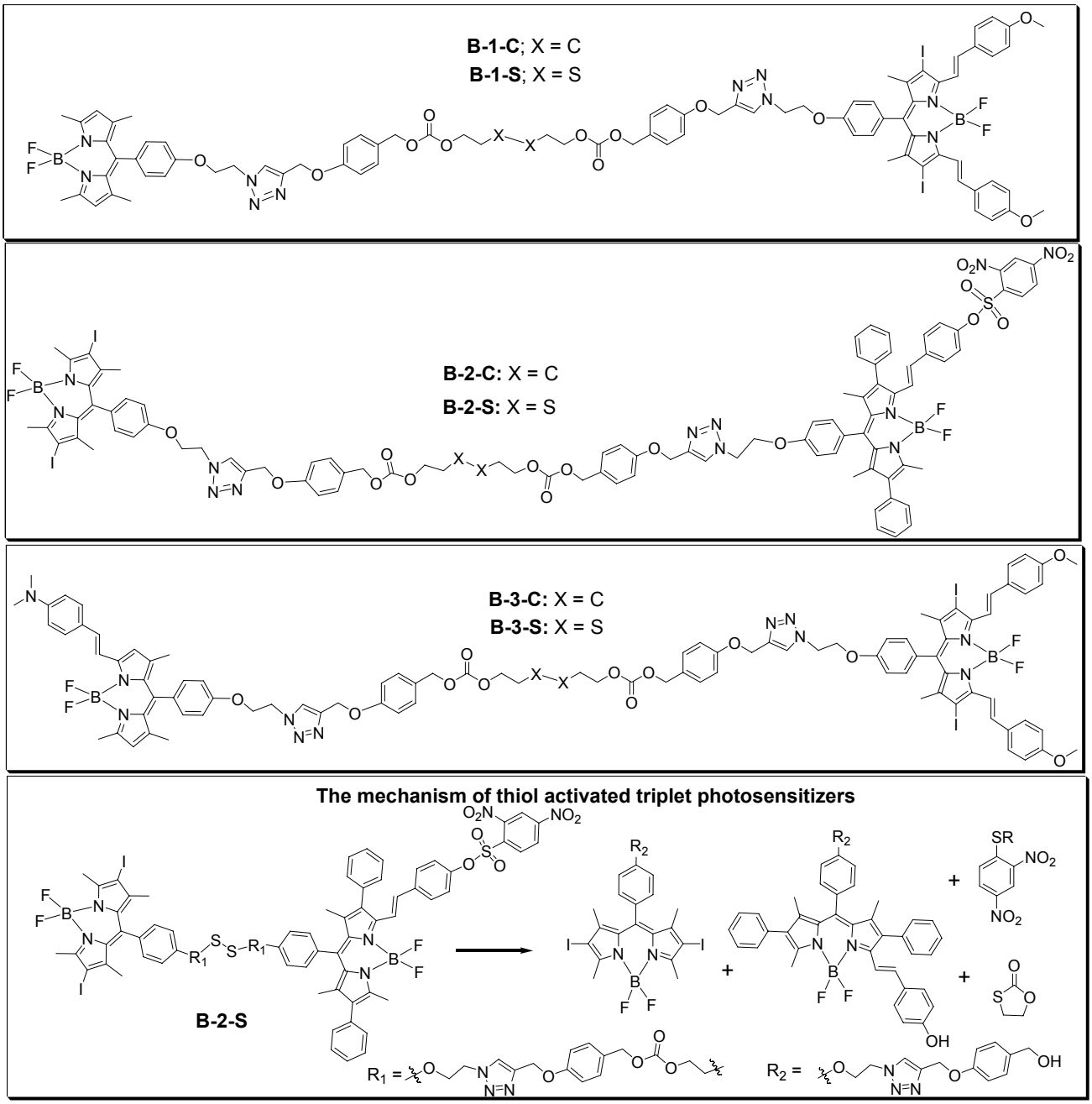

Scheme 1. The thiol-activatable Bodipy-derived dyad triplet photosensitizers used in the study.

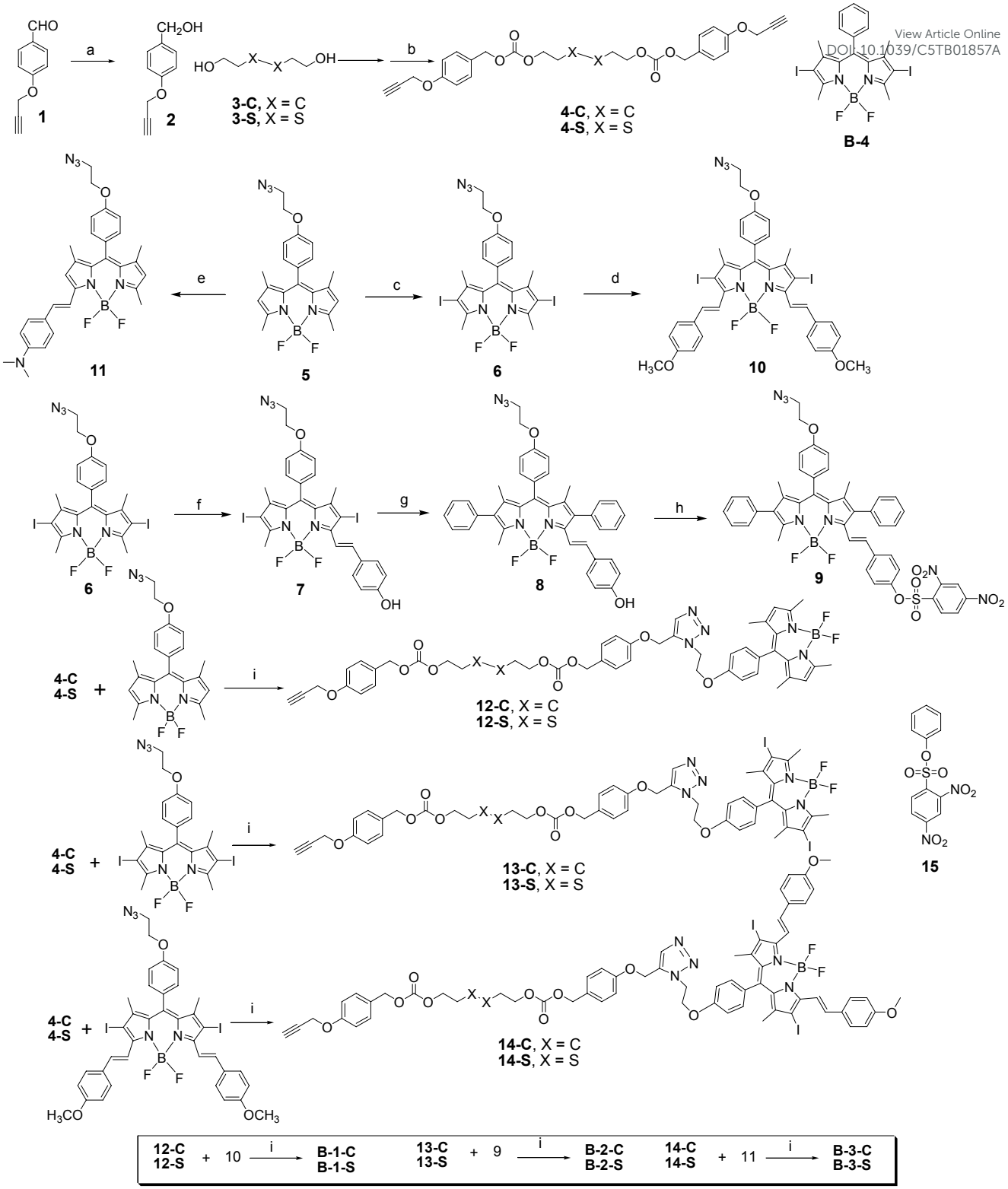

Scheme 2. Preparation of the Dyads. (a) $NaBH_4$, EtOH. (b) Triphosgene, DCM. (c) Iodine, iodic acid, EtOH. (d) 4-Methoxybenzaldehyde, piperidine, acetic acid, toluene. (e) 4-*N,N*-dimethylbenzaldehyde, piperidine, acetic, toluene. (f) 4-Hydroxybenzaldehyde, piperidine, acetic, toluene. (g) Phenyl boronic acid, $Pd(PPh_3)_4$, K_2CO_3, toluene/EtOH/H_2O = 2/2/1 (v/v). (h) 2,4-Dinitrosulfonylchloride, Et_3N, DCM. (i) $CHCl_3$/EtOH/H_2O = 12/1/1 (v/v), $CuSO_4 \cdot 5H_2O$, sodium ascorbate.

Experimental Section

Analytical Measurements

Luminescence lifetimes were measured on a OB920 fluorescence/phosphorescence lifetime instrument. The nanosecond time-resolved transient difference absorption spectra were detected by Edinburgh LP920 instruments (Edinburgh Instruments, UK). The signal was digitized with a Tektronix TDS 3012B oscilloscope and was analyzed by the LP900 software. All samples in flash photolysis experiments were deaerated with N_2 for ca. 15 min before measurement and the gas flow is kept during the measurement.

Synthesis of complex B-1-S

General methods. Under Ar atmosphere, a mixture of compound **12-S** (48.5 mg, 0.04 mmol), **9** (44.7 mg, 0.05 mmol) and $CuSO_4{\cdot}5H_2O$ (0.08 mmol, 8.0 mg) were dissolved in $CHCl_3$/EtOH/H_2O (12/1/1, v/v, 12 mL). Then sodium ascorbate (0.08 mmol, 7.5 mg) was added. The mixture was stirred at room temperature (RT) for 12 h. After completion of the reaction, water (10 mL) was added, the mixture was extracted with dichloromethane (3×30 mL). The organic layer was dried over Na_2SO_4. After removal of the solvent under reduced pressure, the mixture was purified by column chromatography (silica gel, DCM/EtOAc = 5/2, v/v) to give orange solid (41.9 mg). Yield: 51 %. ^{1}H NMR (500 MHz, $CDCl_3$) δ = 8.16 (d, 2H, J = 16.8 Hz), 7.84 (d, 2H, J = 8.4 Hz), 7.62–7.56 (m, 6H), 7.34–7.30 (m, 4H), 7.18–7.15 (m, 4H), 7.00–6.93 (m, 12H), 5.96 (s, 2H), 5.24 (d, 4H, J = 8.0 Hz), 5.09 (d, 4H, J = 4.0 Hz), 4.83–4.77 (m, 4H), 4.46–4.39 (m, 4H), 4.37–4.33 (m, 4H), 3.85 (s, 6H), 2.93–2.89 (m, 4H), 2.54 (s, 6H), 1.46 (s, 6H), 1.38 ppm (s, 6H). ^{13}C NMR (125 Hz, $CDCl_3$) δ = 160.7, 158.6, 158.5, 158.3, 155.4, 154.8, 150.5, 145.6, 144.1, 144.0, 143.0, 141.2, 139.1, 137.9, 133.1, 131.7, 130.4, 129.9, 129.4, 129.3, 128.7, 128.4, 128.1, 127.8, 124.1, 121.1, 116,7, 115.3, 115.0, 114.8, 114.6, 114.3, 82.7, 69.6, 66.3, 66.2, 65.6, 61.9, 55.4, 49.8, 17.8, 14.6.ppm. HRMS (MALDI): m/z calcd for $[C_{84}H_{80}B_2F_4O_{12}N_{10}I_2S_2]^+$: m/z = 1836.3610; found m/z =1836.3622.

Synthesis of complex B-1-C

General methods. Under Ar atmosphere, a mixture of compound **12-C** (23.1 mg, 0.02 mmol), **9** (26.8 mg, 0.03 mmol) and $CuSO_4{\cdot}5H_2O$ (0.05 mmol, 5.0 mg) were dissolved in $CHCl_3$/EtOH/H_2O (12/1/1, v/v, 12 mL). Then sodium ascorbate (0.05 mmol, 4.9 mg) was added. The mixture was stirred at RT for 12 h. After completion of the reaction, water (10 mL) was added. The mixture was extracted with dichloromethane (3×20 mL), the organic layers were dried over Na_2SO_4. After removal of the solvent under reduced pressure, the mixture was purified by column chromatography (silica gel, DCM/EtOAc = 5/2, v/v) to give orange solid (18.5 mg). Yield: 45 %. ^{1}H NMR (500 MHz, $CDCl_3$) δ = 8.15 (d, 2H, J = 15.0 Hz), 7.84 (d, 2H, J = 10.0 Hz), 7.62–7.57 (m, 6H), 7.34–7.31 (m, 4H), 7.19–7.16 (m, 4H), 7.00–6.94 (m, 12H), 5.97 (s, 2H), 5.25 (d, 4H, J = 10.0 Hz), 5.08 (d, 4H, J = 10.0 Hz), 4.84–4.78 (m, 4H), 4.47–4.41 (m, 4H), 4.13–4.09 (m, 4H), 3.86 (s, 6H), 2.54 (s, 6H), 1.65–1.62 (m, 4H), 1.47 (s, 6H), 1.39 (s, 6H), 1.38–1.36 (m, 4H). ^{13}C NMR (125 Hz, $CDCl_3$) 160.9, 158.8, 158.6, 158.5, 155.6, 155.4, 150.6, 145.7, 144.3, 143.2, 141.4, 139.3, 138.1, 133.3, 131.9, 130.5, 130.1, 129.7, 129.6, 129.4, 128.6, 128.3, 124.2, 121.4, 116.9, 155.5, 115.2, 115.0, 114.5, 82.9, 69.4, 68.1, 66.5, 62.1, 55.4, 49.9, 28.7, 25.5, 17.9, 14.8. HRMS (MALDI): m/z calcd for $[C_{86}H_{84}B_2F_4O_{12}N_{10}I_2]^-$: 1800.4482; found m/z = 1800.4457

View Article Online
DOI: 10.1039/C5TB01857A

Synthesis of complex B-2-S

The synthesis is similar to that of **B-1-S**. Black solid. Yield: 21.7 mg (54 %). ^{1}H NMR (500 Hz, $CDCl_3$) δ = 8.65 (d, 1H, J = 5.0 Hz), 8.47–8.45 (m, 1H), 8.11–8.09 (m, 1H), 7.85 (d, 2H, J = 10.0 Hz), 7.62 (d, 1H, J = 20.0 Hz), 7.42–7.36 (m, 5H), 7.34–7.29 (m, 5 H), 7.22–7.20 (m, 3 H), 7.17–7.14 (m, 3 H), 7.07 (d, 2H, J = 10.0 Hz), 6.99–6.94 (m, 8 H), 6.42 (d, 1 H, J = 15.0 Hz), 5.24 (d, 4H, J = 15.0 Hz), 5.09 (d, 4H, J = 5.0 Hz), 4.83–4.80 (m, 4H), 4.46–4.42 (m, 4H), 4.37–4.34 (m, 4H), 2.93–2.90 (m, 4H), 2.63 (s, 6H), 2.56 (s, 3 H), 1.69 (s, 3 H), 1.40 (s, 6 H), 1.36 (s, 3 H). ^{13}C NMR (125 Hz, $CDCl_3$) δ = 167.7, 158.6, 158.4, 156.8, 156.3, 154.9, 150.9, 149.0, 148.4, 148.1, 145.2, 141.0, 140.9, 140.0, 139.4, 137.2, 135.0, 134.8, 134.7, 134.1, 133.2, 132.8, 132.6, 132.3, 131.6, 130.9, 130.4, 130.1, 129.7, 129.4, 128.8, 128.7, 128.6, 128.4, 128.1, 127.9, 127.6, 127.4, 126.4, 122.1, 120.7, 120.3, 115.4, 115.3, 114.9, 114.8, 85.8, 69.5, 66.2, 65.6, 61.6, 60.4, 53.4, 50.2, 37.0, 31.9, 30.6, 29.7, 29.4, 19.2, 17.2, 16.0, 14.1, 13.7, 13.2, 12.6. Determination of mass spectra failed.

Synthesis of complex B-2-C

The synthesis is similar to that of **B-1-C**. Black solid (30.6 mg). Yield: 85 %. ^{1}HNMR (500 MHz, $CDCl_3$) δ = 8.64 (s, 1 H), 8.47–8.45 (m, 1H), 8.11 (s, 1H, J = 10.0 Hz), 7.85 (d, 2H, J = 15.0 Hz), 7.62 (d, 1H, J = 20.0 Hz), 7.42–7.36 (m, 5H), 7.34–7.30 (m, 7H), 7.23–7.20 (m, 4H), 7.17–7.14 (m, 4H), 7.07–7.06 (d, 2H, J = 5.0 Hz), 7.00-6.95 (m, 8H), 6.42 (d, 1H, J = 15.0 Hz), 5.24 (d, 4H, J = 15.0 Hz), 5.08 (d, 4H, J = 10.0 Hz), 4.84–4.79 (m, 4H), 4.46–4.42 (m, 4H), 4.32–4.29 (m, 4H), 2.63 (s, 6H), 2,56 (s, 3H), 1.65-1.63 (m, 4H), 1.40 (s, 6H), 1.39 (s, 6H), 1.36–1.34 ppm (m, 4H). ^{13}C NMR (125 MHz, $CDCl_3$) δ = 158.9, 158.7, 158.6, 156.9, 155.4, 151.1, 149.1, 148.5, 148.3, 145.4, 141.2, 141.1, 140.0, 139.6, 137.3, 135.1, 135.0, 134.8, 134.2, 133.6, 133.5, 133.4, 132.9, 132.8, 132.5, 131.8, 131.1, 130.5, 130.4, 130.2, 129.8, 129.5, 129.0, 128.9, 128.7, 128.6, 128.3, 128.0, 127.8, 127.5, 126.5, 124.2, 122.2, 120.9, 120.4, 115.5, 115.4, 115.0, 114.9, 85.8, 68.1, 66.5, 65.7, 62.1, 50.0, 32.1, 30.7, 29.9, 29.5, 28.7, 25.5, 22.9, 19.4, 17.4, 16.2, 14.3, 13.9, 13.3, 12.8 ppm. Determination of mass spectra failed.

Synthesis of complex B-3-S

The synthesis is similar to that of **B-1-S**. Orange solid (25.5 mg). Yield: 65 %. ^{1}H NMR (500 MHz, $CDCl_3$) δ = 8.15 (d, 2H, J = 15.0 Hz) 7.82 (s, 2H), 7.62–7.57 (m, 6H), 7.50–7.47 (m, 3H), 7.33–7.31 (m, 4H), 7.22–7.14 (m, 5H), 7.00–6.92 (m, 12H), 6.68 (d, 2 H, J = 10.0 Hz), 6.58 (s, 1H), 5.95 (s, 1H), 5.23 (d, 4H, J = 5.0 Hz), 5.09 (s, 4H), 4.80–4.76 (m, 4H), 4.44–4.40 (m, 4H), 4.39–4.33 (m, 4H), 3.86 (s, 6H), 3.01 (s, 6H), 2.92–2.90 (m, 4H), 2.57 (s, 3H), 1.45 (s, 6H), 1.42 (s, 3H), 1.38 ppm (s, 3H). ^{13}C NMR (125 MHz, $CDCl_3$) δ = 160.9, 158.8, 158.7, 158.4, 155.0, 150.6, 145.8, 144.2, 139.3, 138.1, 133.3, 130.5, 130.3, 130.0, 129.9, 129.4, 128.5, 128.0, 124.2, 117.8, 116.8, 115.5, 115.1, 115.0, 82.9, 69.7, 66.5, 66.4, 65.8, 62.1, 55.6, 49.9, 37.2, 29.9, 17.9, 17.4, 15.1, 14.8, 14.7. ppm. HRMS (MALDI): m/z calcd for $[C_{93}H_{89}B_2F_4O_{12}N_{11}S_2I_2]^+$: 1967.4345; found m/z = 1967.4329.

Synthesis of complex B-3-C

The synthesis is similar to that of **B-1-C**. Orange solid (26.1 mg). Yield: 71 %. ^{1}H NMR (500 MHz, $CDCl_3$) δ = 8.15 (d, 2H, J = 15.0 Hz), 7.82 (s, 2H), 7.62–7.57 (m, 6H), 7.50–7.47 (m, 3H), 7.34–7.32 (m, 4H), 7.22–7.15 (m, 5H), 7.00–6.93 (m, 12H), 6.68 (d, 2H, J = 10.0 Hz), 6.58 (s, 1H), 5.95 (s, 1H), 5.24 (d, 4H, J = 5.0 Hz), 5.07 (s, 4H), 4.81–4.77 (m, 4H), 4.45–4.39 (m, 4H), 4.11–4.09 (m, 4H), 3.86 (s, 6H), 3.01 (s, 6H), 2.57 (s, 3 H), 1.64–1.62 (m, 4H), 1.46 (s, 6H), 1.43 (s, 3H), 1.38 (s, 3H), 1.37–1.35 (m, 4H). ^{13}C NMR (125 MHz, $CDCl_3$) δ = 160.9, 158.8, 158.6, 158.5, 155.3, 150.6, 145.7, 144.3, 142.5, 139.3, 138.1, 133.3, 130.5, 130.1, 129.9, 129.7, 129.4, 129.2, 128.5, 128.4, 128.3, 124.2, 117.8, 116.8, 115.5, 115.2, 115.0, 114.5, 82.9, 69.4, 68.1, 66.5, 66.4, 62.1, 55.6, 49.9, 28.7, 25.5, 17.8, 15.0, 14.8 ppm. HRMS (MALDI): m/z calcd for $[C_{95}H_{93}B_2F_4O_{12}N_{11}I_2]^+$: 1931.5217; found m/z = 1931.5236.

Cell Culture and Luminescence Imaging.

Human endometrial carcinoma cell line (Hela) was obtained from School of Life Science and Biotechnology, Dalian University of Technology. HeLa cell line was cultured in Dulbecco's modified Eagle's medium (DMEM) containing 10% fetal bovine serum (FBS), 100 μg mL^{-1} streptomycin and 100 U mL^{-1} penicillin at 37°C in a humidified incubator containing 5% CO_2 and 95% air. After HeLa cells were cultured for 24 hours, the dyads (25 μM) was added and the cells were cultured another 4 hours. Before HeLa cells were observed with confocal laser fluorescence microscopic images, the cells were rinsing three times with PBS buffer solution in order to remove excess dyads.

MTT Assay.

MTT assay was carried out to investigate the dark toxicity and phototoxicity of dyads for cell growth. Hela cells were first seeded to two 24-well plates at a seeding density of 1×10^4 cells per well in 400 μL complete medium, which was incubated at 37 °C for 24 h. After rinsing with PBS, Hela cells were incubated with 400 μL culture media containing serial concentrations of Dyad for 4 h. One plate was kept in the dark for studying dark toxicity, and another plate was irradiated using a 520-530 nm LED at a power of 5W/ m^2 for 15 min. Afterward, the cells were grown for another 24 h. Then, 40 μL of 5 mg mL^{-1} MTT solution in pH 7.4 PBS was added to each well. After 4 h incubation, the medium containing un-reacted MTT was removed carefully, and 400 μL DMSO was added to each well to dissolve the produced blue formazan. After 5 min, the optical density (OD) at a wavelength of 490 nm was measured with Bio-Rad microplate reader. The percentage of growth inhibition was calculated with Eq 7.

$$\text{Growth Inhibition}=\left(1-\frac{\text{OD value of test}}{\text{OD value of control}}\right)\times100 \qquad \textbf{(Eq. 7)}$$

Results and discussion

Molecules Design and Synthesis.

The main goal of the new PDT reagents is to attain the *simultaneously* activated PDT effect and the fluorescent imaging capability, with *different* chromophores in a dyad containing cleavable linker.[19b] To this end, we use the disulfide bond (–S–S–) as a linker between the PDT and the fluorescence modules (**B-1-S**, **B-2-S** and **B-3-S**, Scheme 1). It is known that disulfide bond can be selectively cleaved by thiols such as Cys and GSH.[21,22,24] These reagents may demonstrate targeted PDT effect toward cancer cells or tissues because it is known that the thiol compound concentration is higher than the normal thiols or tissues.[24] At the same time the PDT treatment can be imaged with the activated fluorescence.

In order to achieve efficient PDT and strong fluorescence upon the activation (cleavage by thiol), the PDT reagents were designed as FRET dyads in which the PDT and fluorescence modules were based on separated chromophores (Scheme 1).[18,19] The singlet energy donor and the acceptor were selected in such a way that the PDT module is singlet energy donor, thus the ISC of PDT module can be substantially inhibited by the FRET process (**B-2-S** and **B-2-C**, Scheme 1). The fluorescence of the singlet energy acceptor (the fluorophore) was caged by 2,4-dinitrobenzenesulfonate (DNBS) group.[19a,28–33] Thus the singlet energy acceptor is a caged fluorophore so that the fluorescence can be switched ON by the same stimuli that activate the PDT module, i.e. biological thiols, such as Cys or GSH (Scheme 1). **B-2-S** was designed following these rationales. Bodipy was selected as the fluorophore due to the strong absorption of visible light, high fluorescence quantum yield, good photostability and feasible derivatization.[34–38] The expected PDT properties are as followings, in the absence of thiols, the PDT effect is in OFF state because the ISC of the PDT module is inhibited by the FRET to the styrylBodipy moiety.[39] On the other hand, the fluorophore is a caged by 2,4-dinitrobenzenesulfonyl (DNBS) thus no fluorescence can be observed.[19a,29] In the presence of thiols, the disulfide bond is cleaved, FRET ceased thus the ISC of PDT module is activated, cytotoxic $^1O_2$ will be produced upon photoirradiation. At the same time, the fluorophore will be simultaneously un-caged by cleavage of the DNBS moiety by the thiols, thus the red fluorescence will be switched on concomittantly.[29] Thus **B-2-S** is a thiol-activatable PDT reagents which show activatable fluorescence upon activation to selectively illuminate the $^1O_2$ producing region.[19]

We also designed reference dyads with different FRET/cage strategies to demonstrate **B-2-S** is the optimal (Scheme 1). In **B-1-S**, the fluorophore was caged by FRET. However, the PDT module is *not* caged.[19b] In the presence of thiols and thus cleavage of the disulfide bond, the fluorescence will be switched ON but the $^1O_2$ producing capability is not altered.[12] Thus the switching capability of **B-1-S** is only half to that of **B-2-S**. On the other hand, we used a fluorophore which shows longer absorption wavelength in **B-3-S** than that used in **B-1-S** and **B-2-S**. Similar to **B-1-S**, the PDT module is not caged. However, we found that the fluorescence is very weak either in the absence or presence of thiols, which is due to the intramolecular charge transfer feature.[40]

In order to prove the activation effect with thiols on the photophysical properties, we prepared the references compounds without the disulfide bonds, i.e. the –S–S– linker was replaced with the *un-cleavable* –C–C– linker (**B-1-C**, **B-2-C** and **B-3-C**. Scheme 1).

It should be pointed out that the PDT reagent should show some extent of solubility in aqueous solution. The dyads studied herein are soluble in aqueous solvent (the concentration is up to 1.0×10^{-5} M). However, we did not take much effort to add water-soluble segments to the molecular structure.

The preparation of the six dyads were present in Scheme 2. Firstly the thiol-cleavable and the un-cleavable linkers were prepared with the alkynyl intermediates. Then different fluorescence modules or the PDT modules were consecutively attached to the linkers. All the compounds were obtained in moderate to satisfactory yields.

UV−vis Absorption and Fluorescence Spectra.

The UV−vis absorption spectra of the compounds were studied (Fig. 1). The common feature of the dyads is the dual absorption bands. For example, **B-1-S** shows absorption at 501 nm and 662 nm, respectively (Fig. 1a), which are attributed to the fluorescence module (Bodipy) and the PDT module (iodo-StyrylBodipy part), respectively.[36] These absorption bands are highly identical to those of the reference components of the dyad, thus we propose that there is no significant electronic interaction between the chromophores in the dyad at ground state.[36,41] For **B-2-S**, the absorption at 535 nm and 580 nm is due to the diiodoBodipy and the caged styrylBodipy fluorophore, respectively (Fig. 1b). For **B-3-S**, the absorption of the dimethylaminostyrylBodipy is at 608 nm, the PDT module shows absorption at 656 nm (Fig. 1c).

The variation of the UV−vis absorption spectra of the compounds in presence of thiols were studied. Only minor variation were observed (Fig. 1a−1c). The UV−vis absorption spectra of **B-1-C**, **B-2-C** and **B-3-C** also was studied in the presence of Cys, the change of spectra is no significant (See ESI †, Fig. S48).

The fluorescence of the dyads in the absence of thiols were studied (Fig. 1d-1f). For **B-1-S** alone, weak fluorescence at 513 nm and 699 nm were observed. The weak emission band at 513 nm is due to the quenched emission of the fluorescence module by the FRET effect, whereas the weak fluorescence band at 699 nm is due to the PDT module (efficient ISC).[42] Upon addition of Cys thus the cleavage of the disulfide bond, the FRET ceased in **B-1-S** and the fluorescence of the fluorophore module recovered (enhanced by 9.4-fold). Conversely, the emission at 699 nm decreased, which can be attributed to cease of FRET (λ_{ex} = 475 nm, excitation into the fluorescence module, i.e. the energy donor). For **B-2-S**, the emission of the caged fluorophore enhanced by 28.5-fold in the presence of Cys (Fig. 1e), due to the cleavage of the DNS moiety, an electron trap to quench the fluorophore.[28,29,31,32,43] Thus ratiometric response was observed for **B-1-S** in the presence of Cys, with the I_{513nm}/I_{699nm} varied from 1.8 from 38.3. The separation of the two emission band is as larger as ca. 186 nm. Previously a ratiometric caspase-specific PDT/luminescence imaging reagent was studied with porphyrin as the energy acceptor and rhodamine as energy donor, separation of the two emission band is 90 nm.[12]

We noted the emission at 622 nm of **B-2-S** is slightly red-shifted upon cleavage of the DNS moiety, which is caused by intramolecular charge transfer (ICT) effect.[29] The emission at 554 nm increased slightly upon addition of Cys, which is due to the cease of the FRET effect. The emission band at 554 nm is still very weak upon addition of Cys, which is due to the efficient ISC of this PDT module. For **B-3-S**, the emission band at 695 nm was slightly enhanced upon addition of Cys. This increase upon cleavage of the disulfide bond is due to the ceasing of the intramolecular electron transfer (see later section).[42]

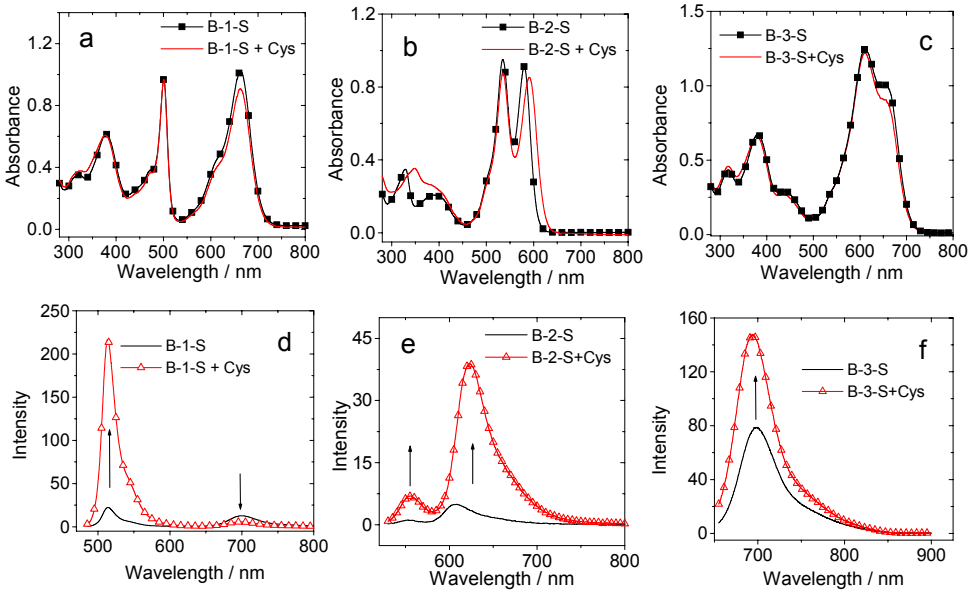

Fig. 1 UV−vis absorption spectra of (a) **B-1-S**, (b) **B-2-S** and (c) **B-3-S** in the presence and in the absence of Cys. The corresponding fluorescence emission spectral changes are presented in (d) **B-1-S** (λ_{ex} = 475 nm), (e) **B-2-S** (λ_{ex} = 520 nm) and (f) **B-3-S** (λ_{ex} = 650 nm). c[Dyads] = 1.0×10^{-5} M, c[Cys] = 3.0×10^{-3} M. In DMF/H_2O = 4/1 (v/v. pH = 7.4), 25 °C.

Table3. Photophysical Parameters of Dyads and the Reference Compounds [a]

	λ_{abs} (nm)	ε / 10^5 M^{-1} cm^{-1} [b]	λ_{em} (nm) [c]	Φ_L(%) [d]	τ_F (ns) [e]	τ_T (μs) [f]	Φ_Δ(%) [g]
10	661	0.98	694	7.0	2.10	1.40	61.2
11	608	0.78	713	2.80	1.20	–	–
B-4	535	0.83	556	2.4	0.13	110.2	78.1
In the absence of Cys							
B-1-S	501/662	0.97/1.02	513/699	5.8	1.58/1.94	1.4	66.8h/69.3[i]
B-1-C	501/662	1.09/1.05	513/699	5.5	1.61/1.97	1.4	62.4h /69.4[i]
B-2-S	535/580	0.96/0.92	610	1.3	2.14	179.9	16.7j/6.3[k]
B-2-C	535/580	0.96/0.92	610	1.1	2.27	152.6	16.1 j/5.9 [k]
B-3-S	608/656	1.24/1.00	694	5.4	1.55	0.91	16.5l
B-3-C	608/655	1.13/0.92	695	5.4	1.59	0.85	15.3l
9	580	0.93	610	1.1	2.07	–	–
In the presence of Cys							
B-1-S	501/663	0.96/0.90	513/699	45.2	4.27/1.96	1.4	22.8 h /61.1[i]
B-1-C	501/664	1.08/0.99	513/699	6.6	1.61/1.98	1.4	59.3h /68.9 [i]
B-2-S	535/591	0.88/0.85	622	47.6	3.93	45.4	71.5 j /6.5[k]
B-2-C	535/592	0.88/0.86	622	42.9	3.91	172.2	19.1j /6.9 [k]
B-3-S	608/654	1.21/0.92	694	6.8	2.08	1.38	59.5l
B-3-C	608/655	1,10/0.90	695	5.2	1.60	0.92	12.8l
9	591	0.86	622	50.1	3.95	–	–

[a] $c = 1.0 \times 10^{-5}$ M in DMF/H_2O (4/1). 25 °C. [b] Molar absorption coefficient at the absorption maxima.ε: 10^5 M^{-1} cm^{-1}. [c] The emission maxima. [d] Fluorescence quantum yields determined with Rhodamine B as standard (Φ_F = 65 % in EtOH). [e] Fluorescence lifetime. [f] Triplet excited state lifetime. [g] Singlet oxygen ($^1O_2$) quantum yield. [h] Recorded upon excitation at 500 nm. [i] Recorded upon excitation at 665 nm. [j] Recorded upon excitation at 535 nm. [k] Recorded upon excitation at 580 nm. [l] Recorded upon excitation at 665 nm.

The reference dyads with the un-cleavable C–C linker were also studied. For **B-1-C** and **B-3-C**, no fluorescence enhancement was observed. For **B-2-C**, fluorescence enhancement was observed due to the cleavage of the DNS from the caged fluorophore (Fig. S49).

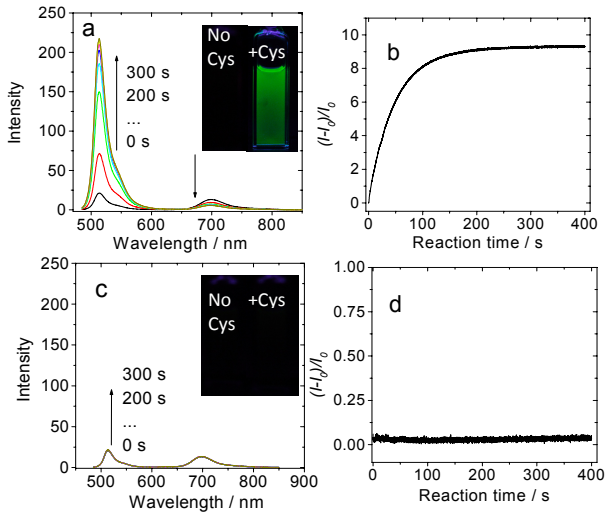

Fig. 2 (a) The change of fluorescence of **B-1-S** in presence of Cys, (b) The kinetics of **B-1-S** in presence of Cys. (c) and (d) The change of fluorescence and the kinetics in different time in presence of Cys for **B-1-C**, λ_{ex} = 475 nm. c[Dyads] = 1.0×10^{-5} M, c[Cys] = 3.0×10^{-3} M in H_2O/DMF (1/4, v/v), pH = 7.4, 25 °C. Photograph was taken under hand-hold UV lamp irradiation (λ_{ex} = 365 nm).

The kinetic of the response of dyads to Cys, i.e. the cleavage kinetics, was monitored by following the fluorescence variation. For **B-1-S**, the emission intensity at 513 nm increased with elapse of the time after addition of Cys (Fig. 2a). The response is fast (Fig. 2b).[44] Fast kinetics was observed k = 0.13±0.04 s^{-1}. For **B-1-C**, however, no fluorescence enhancement was observed in the presence of Cys because the linker is unable to be cleaved by Cys. Thus the function of the thiol-activation fluorescence was achieved with **B-1-S**.

Similar studies were carried out for **B-2-S** (Fig. 3). Upon addition of Cys, thus cleavage of the DNS moiety from the styrylBodipy, the uncaged fluorophore give strong fluorescence emission in red spectral region (Fig. 3a),[29] which is different from that of **B-1-S** that gives green fluorescence upon activation. Fast kinetics was observed with $k = 1.85 \pm 0.03$ s^{-1} for **B-2-S** (Fig. 3b), which is much faster than that of **B-1-S**. This result can be rationalized by the different caging mechanism for the fluorescence, in **B-1-S**, it is the cleavage of the disulfide bond, but in **B-2-S** it is the cleavage of the DNS moiety that switch on the fluorescence (Scheme 1).

Minor fluorescence enhancement (1.21-fold) was observed for **B-3-S** in the presence of Cys (See ESI †, Fig. S52). For **B-3-C**, however, no such enhancement was observed.

In order to study the FRET effect in the absence and in the presence of Cys, the fluorescence excitation spectra of the dyads were investigated (Fig. 4).[45,46] For **B-1-S**, intense excitation band at 513 nm was observed (Figure 4a), where the fluorescence module gives strong absorption. Thus, FRET exists in **B-1-S**. In the presence of Cys, the disulfide linker was cleaved, the intense band at 498 nm in the excitation spectrum disappeared (Fig. 4a), indicated that the FRET ceased. For the dyad with un-cleavable C–C linker, however, no such change was observed (Fig. 4b), indicate that the FRET is persistent in the presence of Cys.

Similarly, two excitation bands were observed for **B-2-S** (Fig. 4c), indicates the FRET from the diiodoBodipy to the caged styrylBodipy fluorophore. In the presence of Cys, thus the cleavage of the disulfide bond, the FRET ceased and the excitation band at 535 nm disappeared (Fig. 4c). For **B-2-C**, i.e. the dyad with the un-cleavable linker, no such change was observed (Fig. 4d). Similar study was applied to the excitation spectra of **B-3-S**. Two excitation bands at 608 nm and 665 nm were observed for **B-3-S** (Fig. 4e), which are due to the fluorophore module and the PDT module, respectively. Thus

FRET from the fluorophore to the PDT module exists. In the presence of Cys, the FRET ceased and the excitation band at 608 nm disappeared. No such change was observed for **B-3-C** (Fig. 4f).

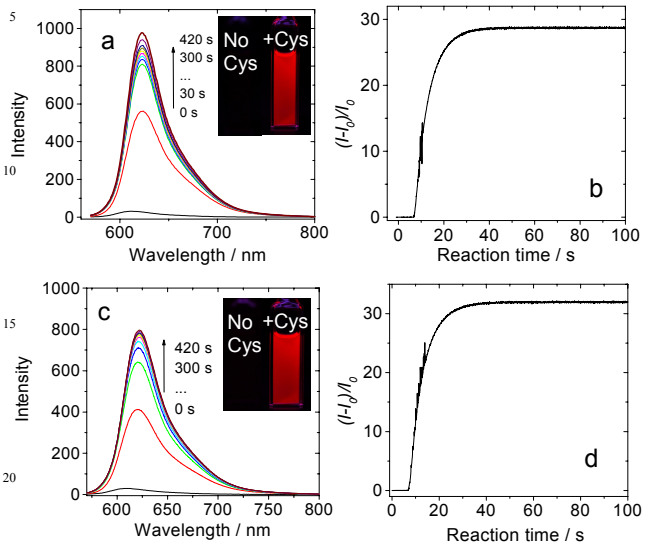

Fig. 3 (a) The change of fluorescence of **B-2-S** in the presence of Cys, (b) The kinetics of **B-2-©S** in presence of Cys. (c) and (d) The change of fluorescence and the kinetics in different time in presence of Cys for **B-2-C**, Photograph was taken under hand UV lamp irradiation (λ_{ex} = 365 nm). *c*[Dyads] = 1.0 × 10^{-5} M, *c*[Cys] = 3.0 × 10^{-3} M, λ_{ex} = 560 nm, in H_2O/DMF (v/v, 1/4), pH = 7.4, 25 °C.

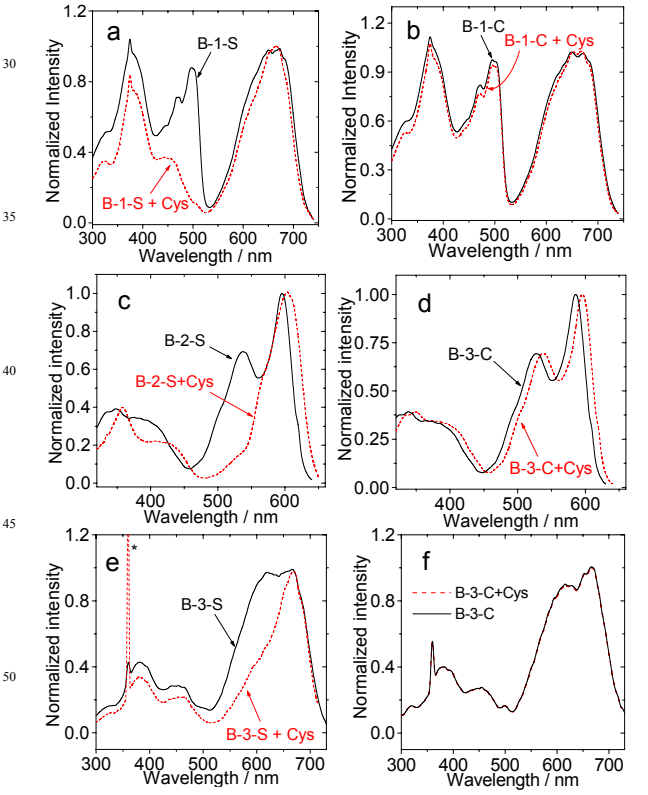

Fig. 4 The change of the fluorescence excitation spectra of **B-1-S**, **B-1-C** and **B-2-S** in the presence of Cys. (a) **B-1-S** (λ_{em} = 750 nm). (b) **B-1-C** (λ_{em} = 750 nm). (c) **B-2-S** (λ_{em} = 640 nm). (d) **B-2-C** (λ_{em} = 640 nm). (e) **B-3-S** (λ_{em} = 720 nm). (f) **B-3-C** (λ_{em} = 720 nm). *c* [Dyads] = 1.0 × 10^{-5} M and *c*[Cys] = 3.0 × 10^{-3} M in H_2O/DMF (v/v =1/4), 25 °C.

The selectivity of the dyads toward different thiols was studied (Fig. 5). The dyads give strong response to the analytes containing -SH group.[47] Thus the dyads **B-1-S** and **B-2-S** can be used as probe for biological thiols. For **B-3-S**, however, only weak fluorescence enhancement was observed in the presence of thiols.

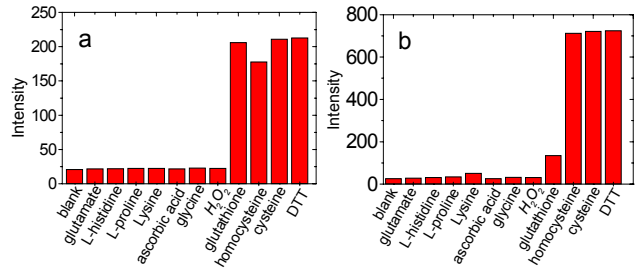

Fig. 5 (a) Response of **B-1-S** to different analytes. Relative fluorescence intensity of 10μM **B-1-S** at 511nm (λ_{ex} = 475 nm) before and after incubation in presence of 3 mM analytes. (b) Response of **B-2-S** to different analytes. Relative fluorescence intensity of 10 μM **B-2-S** at 622 nm (λ_{ex} = 560 nm) before and after incubation in the presence of 3 mM analytes. 25 °C.

Nanosecond transient absorption spectroscopy: switching of the triplet excited state by thiols

Previously pH- or enzyme-activatable PDT reagents were reported, but the variation of the triplet excited states of the compounds were not studied in detail with nanosecond time-resolved transient difference absorption spectroscopy.[7,19b,48] Herein the change of the triplet excited state property of the activatable PDT dyads was investigated with the nanosecond transient difference absorption spectroscopy.

For **B-1-S**, bleaching band at 665 nm was observed upon 640 nm nanosecond laser excitation (Fig. 6c). The lifetime of this transient was determined as 1.8 μs (in toluene), which was substantially reduced to 1.4 ns in aerated solution, indicating that the transient is due to triplet excited state. Since the PDT module in **B-1-S** shows strong steady absorption at 640 nm, the triplet state is localized on the PDT module,[41,49] due to its lower T_1 state energy level than the fluorescence module in **B-1-S**. Selective excitation into the fluorescence module in **B-1-S** (λ_{ex} = 504 nm) gives a very similar transient absorption spectra (Fig. 6a).

Notably the optical density of the spectra upon 504 nm excitation is larger than that upon 640 nm excitation (Fig. 6e). This result is due to the FRET effect in **B-1-S**,[41,50] i.e. the triplet state of the singlet energy acceptor can be produced upon selective excitation into the energy donor. In order to unambiguously prove the FRET, the TA spectra of **B-1-S** upon excitation at 504 nm and 640 nm was compared with that of compound **10** (Fig. 6e and 6f. The reference structure of the PDT module in **B-1-S**). The results show that the spectrum of **10** upon 640 nm excitation is with larger OD values than that upon 504 nm excitation. This result is reasonable since **10** shows stronger absorption at 640 nm than at 504 nm. For dyad **B-1-S**, however, the optical density (OD) values of the spectrum recorded upon 640 nm is weaker than that with 504 nm excitation (Fig. 6e). Thus FRET exists for **B-1-S**, i.e. the FRET following the selective excitation into the fluorescence module of **B-1-S** will convey the energy to the PDT module, and the ISC of the PDT module will produce the triplet state.[49]

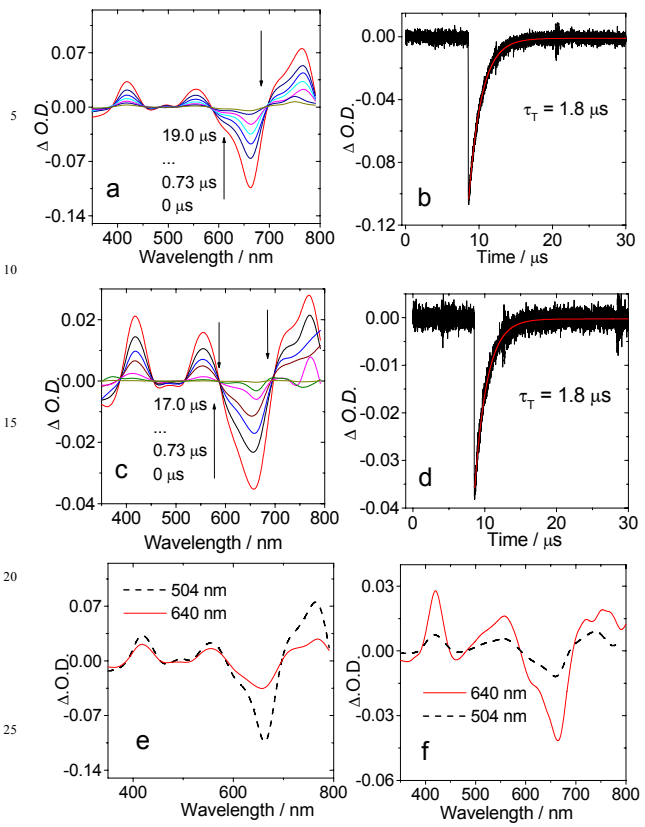

Fig. 6 Nanosecond time-resolved transient difference absorption spectra of **B-1-S** upon excitation at different wavelength. (a) Transient difference absorption spectra and (b) the corresponding decay trace at 660 nm, upon excitation at λ_{ex} = 504 nm; (c) transient difference absorption spectra and (d) the corresponding decay trace at 660 nm. upon excitation at λ_{ex} = 640 nm. (e) Comparison of the TA spectra of **B-1-S** recorded at different excitation wavelengths. The delay time is 0 μs, (f) Comparison of the TA spectra of compound **10** recorded at different excitation wavelengths. The delay time is 0 μs. c[Dyad] = 1.0 × 10^{-5} M in deaerated toluene, 25 °C.

Upon addition of Cys, thus cleavage of the dyad, the TA spectra do not show any substantial change, except the OD value decreased (Fig. 7a and 7b), due to the cease of FRET. The triplet state lifetime remains the same (1.4 μs. In DMF/H_2O = 4/1, v/v). It is the same with triplet state lifetime **10** in DMF/H_2O (Fig. S59). The variation of the OD values upon 504 nm excitation in the presence of Cys was studied (Fig. 7e). It was found the OD value decreased upon cleavage, which supports the FRET postulation.

The change of the triplet excited state manifold of **B-2-S** was also studied with the nanosecond time-resolved transient absorption spectra (Fig. 8). Upon selective excitation into the PDT module (the singlet energy donor in the dyad), triplet excited state localized on the caged fluorescence module was observed, with bleaching band at 584 nm (Fig. 8a). The triplet state lifetime was determined as 179.9 μs (Fig. 8b). No triplet state can be observed with the caged fluorophore (compound **9**) alone with excitation at 585 nm (See ESI †, Fig. S60). Thus the triplet state energy transfer in **B-2-S** was confirmed. It should be pointed out that the triplet state yield of **B-2-S** is low (approximated with the $^1O_2$ quantum yield, Φ_Δ = 16.7%), due to the competition of FRET with the ISC of the PDT module.[18]

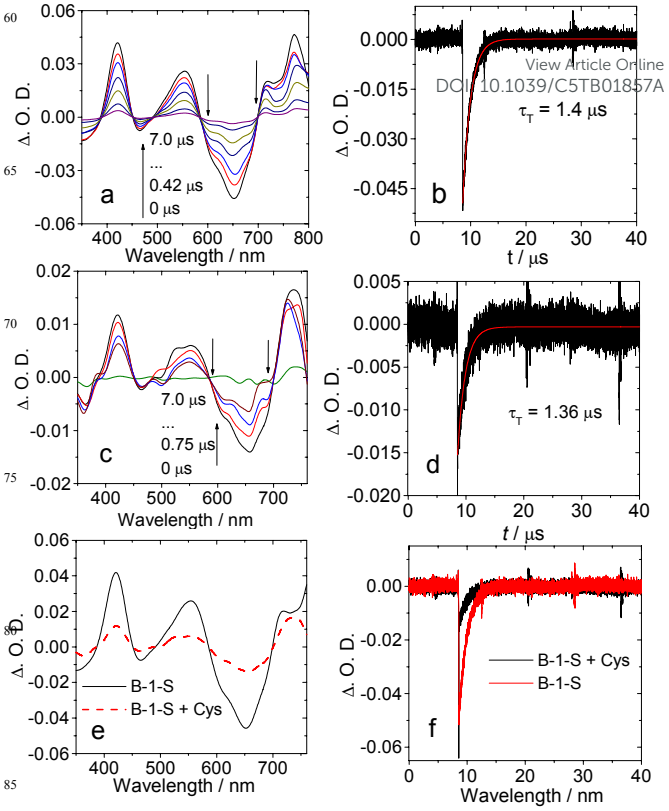

Fig. 7 Nanosecond time-resolved transient difference absorption spectra of **B-1-S** in the presence of Cys. (a) **B-1-S** alone and (b) the decay trace at 660 nm. (c) Transient absorption spectra of **B-1-S** with Cys added and (d) the decay trace at 660 nm. (e) Comparison of the transient absorption spectra of **B-1-S** and **B-1-S** + Cys with delay time of 0 μs and (f) the corresponding decay traces at 660 nm. λ_{ex} = 504 nm. In deaerated DMF/H_2O = 4/1 (v/v). c[Dyad] = 1.0 × 10^{-5} M, c(Cys) = 3.0 × 10^{-3} M, 25 °C

Upon addition of Cys, interesting TA spectral profile was observed (Fig. 8c). For the mixture of **B-2-S** with Cys, i.e. the cleaved dyad, two bleaching band at 535 nm and 590 nm were observed upon nanosecond pulsed laser excitation (Fig. 8c). Furthermore, the transient at 535 nm decrease on the microsecond time scale, and the bleaching band at 591 nm increase concomitantly. Thus we postulate the exist of the *intermolecular* triplet state energy transfer.[51,52] Moreover, the transient bleaching at 591 nm was intensified firstly, which indicated the accumulation of the triplet state of the un-caged fluorophore of **B-2-S**. Then after ca. 30 μs, the transient bleaching decreased, which is due to the decay of the triplet excited state of the un-caged fluorophore. The rate of intermolecular energy transfer was calculated as 2.84 ×10^4 s^{-1} with Eq. 1 and energy transfer efficiency was calculated as 82.4% (Eq. 2).[51] It should be pointed out that investigation on the *intermolecular* triplet excited energy transfer is rare.[52] The efficient intermolecular EnT, facilitated by the long-lived triplet state of the energy donor, will he helpful for the study of intermolecular energy transfer and artificial photosynthetic studies.

$$k_{EnT} = \frac{1}{\tau_2} - \frac{1}{\tau_1} \qquad \textbf{(Eq. 1)}$$

$$\Phi_{EnT} = 1 - \frac{\tau_2}{\tau_1} \qquad \textbf{(Eq. 2)}$$

The response of **B-2-C** to the presence of Cys was studied with TA spectra. The triplet state lifetime of **B-2-C** is 152.6 μs (Fig. 9a and 9b). In the presence of Cys, the TA spectra do not change, the lifetime of the triplet excited state was slightly extended to 172.2 μs (Fig. 9c and 9d). Interestingly, no bleaching band of the PDT module was observed, which indicated that the intramolecular EnT is persistent in the presence of Cys, which is consistent with the fact that the linker between the fluorophore and the PDT module was not cleaved. Thus, no intermolecular triplet energy transfer was observed. As a further proof, the TA spectra of **B-2-C** and **B-2-C**+Cys show the same OD value upon selective excitation into the EnT donor (Fig. 9e).

The transient absorption of **B-3-S** in the absence and in the presence of Cys were also studied. The bleaching band indicate that the triplet state is localized on the PDT module (Fig. 10).[53–55] The lifetime was determined as 0.94 μs. Upon addition of Cys, the TA spectral feature did not change, the lifetime was slightly extended to 1.39 μs. The extension of the triplet state lifetime may be due to the elimination of the intramolecular electron transfer in **B-3-S**.

In order to prove the electron transfer (ET) in **B-3-S**, we compared the TA spectra of **B-3-S** and compound **10** in solvents with different polarity, because it is known that ET is dependent on the solvent polarity.[56–60] In DMF/H_2O = 4/1 (v/v), the OD values of the **B-3-S** spectra is smaller than that of compound **10** upon selective excitation into the singlet energy donor module (Fig. S59), indicating intramolecular electron transfer. In nonpolar solvent such as toluene, the OD value of the compound **B-3-S** and compound **10** are the same. Very close triplet state lifetimes of 1.78 μs and 1.74 μs were observed. These results show that electron transfer is repressed in nonpolar solvent.

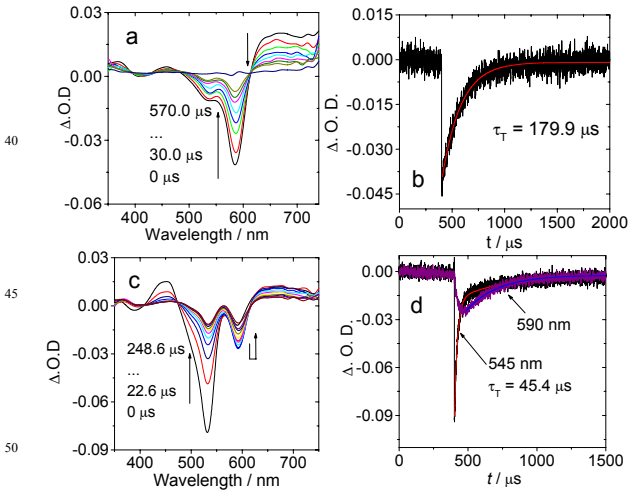

Fig. 8 Nanosecond time-resolved transient difference absorption spectra of **B-2-S** in the presence of Cys. (a) Transient difference absorption spectra of **B-2-S** alone and (b) the decay trace at 580 nm. (c) Transient difference absorption spectra of **B-2-S** with Cys added and (d) the decay trace at 545 nm and 590 nm. In deaerated DMF/H_2O = 4/1 (v/v). Excited with nanosecond pulsed laser at λ_{ex} = 535 nm, c[Cys] = 3.0 × 10^{-3} M, c [Dyad] = 1.0 × 10^{-5} M, 25 °C

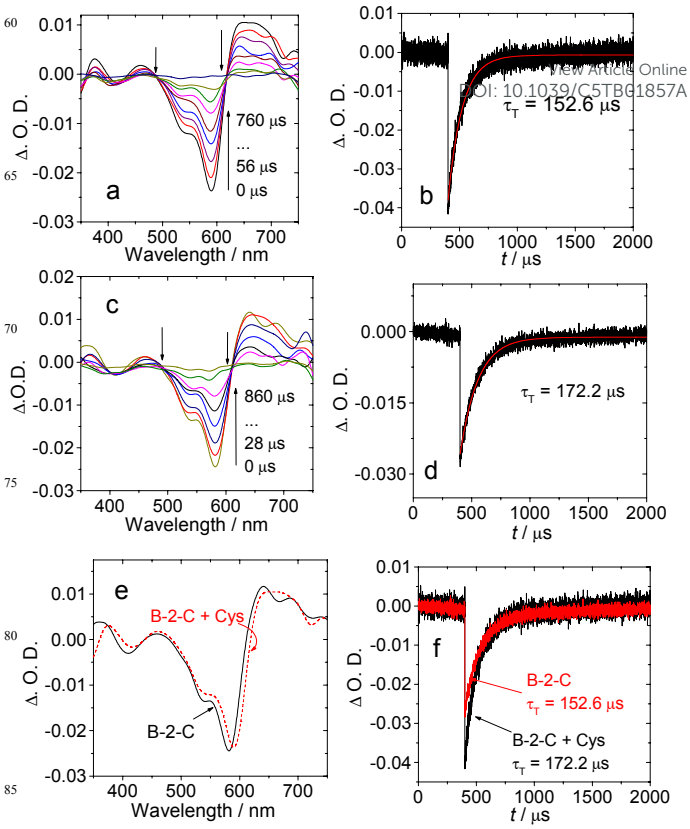

Fig. 9 Nanosecond time-resolved transient difference absorption spectra of **B-2-C** in the presence of Cys. (a) Transient difference absorption spectra of **B-2-C** alone and (b) the decay trace at 580 nm. (c) Transient difference absorption spectra of **B-2-C** + **Cys** and (d) the decay trace at 590 nm. (e) Comparison of the transient difference absorption spectra of **B-2-C** and **B-2-C** + Cys. The decay time is 0 μs and (f) the corresponding decay trace at 590 nm of the two samples. λ_{ex} = 535 nm (nanosecond pulsed laser). C(Cys) = 3.0 × 10^{-3} M and c[Dyads]= 1.0 × 10^{-5} M in deaerated DMF/H_2O = 4/1 (v/v), pH = 7.4, 25 °C.

In order to study intramolecular energy transfer for Bodipy dyads, the rate constants of energy transfer (k_{EnT}) and electron transfer (k_{ET}) were estimated using fluorescence quantum yields and fluorescence lifetimes of the dyads and the energy donor/acceptors (Table 2 and Eq3 and Eq 4).[57] For **B-1-S** and **B-2-S** , k_{EnT} is faster than k_{ET}, so the intramolecular electron transfer can not quench triplet state. But for **B-3-S**, It is not neglect to triplet excited state quenching because of k_{ET} is larger than k_{EnT}.[57] The result is consistent with nanosecond time resolved the transient absorption.

$$k_{ET} = \left[\frac{\Phi_{F(\text{electron accptor part})}}{\Phi_{F(\text{target molecule})}}\right] / \tau_{(\text{electron accptor part})} \qquad \textbf{(Eq. 3)}$$

$$k_{EnT} = \left[\frac{\Phi_{F(\text{energy donor part})}}{\Phi_{F(\text{target molecule})} - 1}\right] / \tau_{(\text{energy donor part})} \qquad \textbf{(Eq. 4)}$$

where k_{ET} is the rate of intramolecular electron transfer, Φ_F (electron acceptor part) and Φ_F(target molecule) are the

fluorescence quantum yields of electron acceptor part and the target molecule and τ (electron acceptor part) is the electron accept part fluorescence lifetime. k_{EnT} is the rate of intramolecular energy transfer constants, Φ_F (energy donor part) and Φ_F (target molecule) are the fluorescence quantum yields of energy donor part and the target molecule and τ (energy donor part) is the energy donor part fluorescence lifetime.

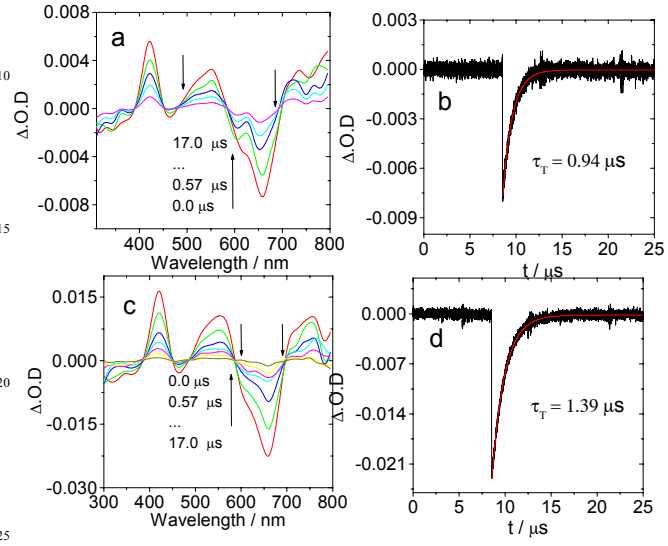

Fig. 10 Nanosecond time-resolved transient difference absorption spectra of (a) **B-3-S** and (b) the corresponding decay trace at 665 nm (c) Transient difference absorption spectra of **B-3-S** + **Cys** and (d) the corresponding decay trace at 665 nm. λ_{ex} = 655 nm, nanosecond pulsed laser. In deaerated DMF/H_2O = 4/1 (v/v). *c*[Dyads] = 1.0 × 10^{-5} M, *c*[Cys] = 3.0 × 10^{-3} M, pH = 7.4, 25 °C.

Table 2. Parameters of Fluorescence Quantum Yield and Fluorescence Lifetimes

	Φ_F (electron accepter)	Φ_F (energy donor)	τ_F (electron accepter)	τ_F (energy donor)	Φ_F (target molecule)	k_{ET} (s^{-1})[d]	k_{EnT} (s^{-1})[e]
B-1-S[a]	7.0%	72.0%	1.91 ns	3.86 ns	5.8%	6.3×10^8	3.2×10^9
B-2-S[b]	1.4%	2.7%	1.86 ns	0.13 ns	1.3%	5.8×10^8	8.3×10^9
B-3-S[c]	7.0%	7.0%	1.91 ns	1.91 ns	5.4%	6.8×10^8	1.6×10^8

[a] the electron acceptor part is 2I-distylBodipy part, energy donor part is Bodipy part. [b] the electron accepter part is StyrylBodipy-DNS part, energy donor part is diiodoBodipy part. [c] the electron accepter part is 2I-distylBodipy part, energy donor part is 2I-distylBodipy part . [d] k_{ET} is the rate of intramolecular electron transfer constants. [e] the rate of intramolecular energy transfer constants.

Electrochemical Studies: the Cyclic Voltammetry and the Free Energy Changes of the Intramolecular Electron Transfer.

The cyclic voltammetry of **B-1-S**, **B-2-S** and **B-3-S** were studied (Fig. 12). For **B-2-S**, two irreversible oxidation waves at +0.82 V and +1.04 V were observed. From the cathodic scan, four irreversible reduction waves were also observed at −0.82 V, −1.15 V, −1.28 V and −1.53V. The control compounds **9**, **15** and **B-4** were also studied (Fig. 12). The Gibbs free energy (ΔG^0_{CS}) of the intramolecular electron transfer were calculated by Weller equation. For example, in **B-2-S**, the caged PDT module is electron donor and the DNS as electron acceptor. With the singlet excited state of diiodoBodipy part as $E_{0,0}$, ΔG^0_{CS} was calculated as −0.44 eV (in DCM), and the ΔG^0_{CS} value was calculated as −0.69 eV in DMF/H_2O (4:1, v/v). It is known that intramolecular electron transfer is favourable in polar solvent. With the triplet excited state of diiodoBodipy part as $E_{0,0}$, ΔG^0_{CS} was calculated as +0.22 eV (in DCM), and ΔG^0_{CS} was calculated as −0.032 eV in DMF/H_2O (4:1, v/v). The energy level of the charge transfer state also was calculated. E_{CTS} is 1.77 eV in DCM, and E_{CTS} is 1.52 eV in DMF/H_2O. However, the triplet state energy level of the caged fluorophore module (1.24 eV, by DFT calculation) is lower than charge transfer state. Therefore the effect of intramolecular electron transfer on the triplet state is not significant.[56–60]

For **B-3-S**, the electron donor moiety is 4-*N*,*N*-dimetylstylBodipy part because of the high oxidation potential (+0.35 V). Large driving force (ΔG^0_{CS} = −0.76 eV in DMF/H_2O) and lower charge transfer state (CTS) energy level were found (1.09 eV). Thus the triplet state can be quenched by the electron transfer.

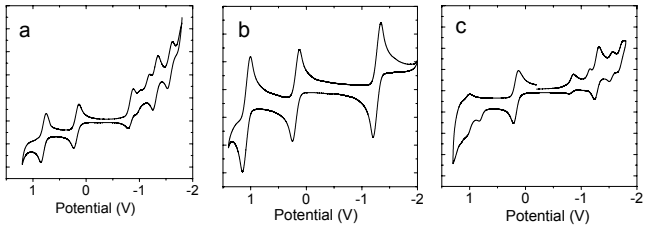

Fig. 12 Cyclic voltammogram of (a) **9**, (b) **B-4**, (c) **B-2-S**. Ferrocene (Fc) was used as internal reference ($E_{1/2}$ = +0.64 V (Fc^+/Fc) vs. standard hydrogen electrode). In deaerated CH_2Cl_2 solutions with 0.10 M Bu_4NPF_6 as supporting electrode, Ag/$AgNO_3$ reference electrode, Scan rates: 0.1 V/s.

Table 3. Redox Potentials of Thiol-Activatable Dyads for Study. Anodic and Cathodic Peak Potential Were Presented. The Potential Values of the Compounds Are Vs. Saturated Calomel Electrode [a]

	$E_{(Ox)}$ (V)	$E_{(Red)}$ (V)
9	+0.79	−0.83, −1.18, −1.30, −1.57
10	+0.67, +0.99	−1.09
11	+0.34, +0.66	−1.44
Bodipy	+0.94	−1.50
15	–[b]	−0.84, −1.28, −1.52
B-4	+1.08	−1.27
B-1-S	+0.70, +1.00	−1.07, −1.51
B-2-S	+0.82, +1.04	−0.82, −1.15, −1.28, −1.53
B-3-S	+0.35, +0.68, +0.92, +1.00	−1.08, −1.43

[a] Cyclic voltammetry in N_2 saturated CH_2Cl_2 containing a 0.10 M Bu_4NPF_6 supporting electrolyte; Counter electrode is Pt electrode; working electrode is glassy carbon electrode; Ag/$AgNO_3$ couple was used as the reference electrode. *c* [Ag^+] = 0.1 M. 20 °C. Conditions: 0.5 mM photosensitizers in CH_2Cl_2, 20 °C. Calculate relative to SCE (saturated calomel electrode). [b] Not observed.

The photophysical process of **B-1-S** was summarized in Scheme 3. In the absence of thiols, fluorescence FRET from the Bodipy to bis(4-methoxy distyryl)-2,6-diiodo-Bodipy leads to the fluorescence quenching of Bodipy part. Moreover, the T_1 state energy level of the Bodipy part level (1.52 eV),[4] is higher than that of the PDT module (1.18 eV by DFT calculation), therefore the triplet excited state is located on the PDT module. The charge

transfer state (CTS) is with energy level of 1.73 eV, thus the fluorescence of the PDT module in **B-1-S** was quenched as compared with that of reference **10** (Table 1). The energy diagram also shows that the triplet state of **B-1-S** should be close to that of compound **10**. The TA spectroscopy demonstrated that this is exact the case (triplet state lifetime of 1.30 μs and 1.40 μs were observed for compound 10 and **B-1-S**, respectively). In the presence of thiols, disulfide bond was cleaved, and FRET ceased, as a result the strong fluorescence of the fluorescence module was observed (Scheme 3b).

The photophysical processes of **B-2-S** were summarized in Scheme 4. In the absence of thiols, upon photoexcitation into the PDT module (2,6-diiodo-Bodipy moiety), the FRET and the ISC will compete with each other. It is known that the ISC of the diiodoBodipy takes about 100 ps, thus the FRET process (takes a few ps) is much faster than the ISC. As a result, the triplet state yield of **B-2-S** will be low, which was proved by the singlet oxygen ($^1O_2$) photosensitizing (Φ_Δ = 16.7%). The fluorescence of 4-hydroxyl styryl 2,6-phenyl-Bodipy part was quenched by

Table 4. The Thermodynamic Driving Force for Photoinduced Electron Transfer Was Calculated From the Weller Equation [a]

	ΔG^0_{CS} [b] (eV)	ΔG^0_{CS} [c] (eV)	E_{CTS} [b] (eV)	E_{CTS} [c] (eV)
B-1-S	−0.43 [d]	−0.68 [d]	1.98	1.73
	+0.46 [e]	+0.21 [e]		
B-2-S	−0.44 [d]	−0.69 [d]	1.77	1.52
	+0.22 [e]	−0.032 [e]		
B-3-S	−0.51 [d]	−0.76 [d]	1.34	1.09
	+0.10 [e]	−0.15 [e]		

[a] Photoinduced electron transfer from energy donor to energy acceptor, ΔG^o_{CS} was calculated by Weller approach and $E_{CTS} = E_{OX} - E_{RED} + \Delta G_s$ and ΔG_S is he static Coulombic energy. [b] in DCM. [c] in DMF/H_2O = 4/1 (v/v). [d] The S_1 state of energy donor as $E_{0,0}$. [e] The T_1 state of energy donor as $E_{0,0}$

2,4- dinitrosulfonyl group (Φ_F = 1.3%). TTET from 2,6-diiodo-Bodipy to 4-hydroxyl styryl 2,6-phenyl-Bodipy part was observed because the triplet excited state level of 4-hydroxyl styryl 2,6-phenyl-Bodipy part (1.24 eV, by DFT calculation) is lower than the PDT module (1.50 eV).[4]

In the presence of thiols (Fig. 4b), both the 2,4-dinitrobenzenesulfonyl group and disulfide bond were cleaved. As a result, strong red fluorescence of the fluorescence module was observed (Φ_F = 47.6%). At the same time, the ISC of the PDT module was recovered due to the cease of the FRET effect (Φ_Δ = 71.5%). Moreover, due to the long triplet excited state lifetime of PDT module (i.e. the 2,6-diiodo-Bodipy moiety), intermolecular triplet excited state energy transfer (TTET) from the (cleaved) PDT module to the uncaged fluorescence module is not negligible. Our results will shed light on new approaches to modulate triplet excited states of organic chromophores.

Switching of the Singlet Oxygen ($^1O_2$) Production by Thiols

The switching of the singlet oxygen ($^1O_2$) photosensitizing ability of the dyads was studied. $^1O_2$ scavenger 1,3-diphenylbenzofuran (DPBF) was used to follow the $^1O_2$ photosensitizing kinetics.

Upon reaction with $^1O_2$, the absorption of DPBF at 414 nm decreased. Firstly, the $^1O_2$ photosensitizing of **B-1-S** upon selective excitation into the Bodipy moiety was compared with that in the presence of Cys (λ_{ex} = 500 nm, Fig. 13a). It was found that upon addition of Cys, the $^1O_2$ photosensitizers ability decreased. The $^1O_2$ quantum yield decreased from 66.8 % to 22.8 %. This is due to the ceased FRET upon cleavage of the S–S linker by thiols, thus the termination of FRET, as a result, the excitation energy harvested by the Bodipy moiety can not be conveyed to the PDT module. No variation of the $^1O_2$ photosensitizing was observed for **B-1-S** upon selective excitation into the PDT module (664 nm. Fig. 13d). This result is reasonable since the ISC of the PDT module in **B-1-S** will not be altered by the cleavage of the linker between the PDT module and the fluorescence module. **B-1-C** gives no response to the presence of Cys (λ_{ex} = 500 nm. See ESI †, Fig. S78).

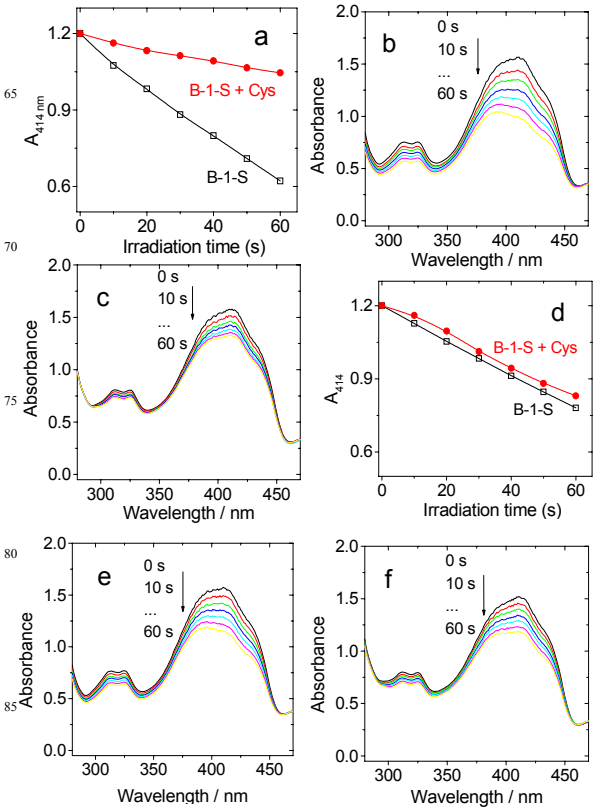

Fig. 13 Switching of the singlet oxygen ($^1O_2$) photosensitizing ability of the dyads by Cysteine. The decreasing of the absorption of $^1O_2$ scavenger 1,3-diphenylisobenzofuran (DPBF) at 414 nm was monitored upon the monochromic light irradiation, with **B-1-S** as photosensitizer. (a) Absorbance of DPBF at 414 nm changes in the absence and in the presence of Cys (λ_{ex} = 500 nm). The UV−vis absorption spectra in the absence (b) and (c) in the presence of Cys. (d), (e) and (f) the corresponding change with **B-1-S** as photosensitizer (λ_{ex} = 664 nm). c [photosensitizers] = 1.0 × 10^{-5} M, c[Cys] = 3.0 × 10^{-3} M, in H_2O/DMF (1/4, v/v), pH = 7.4, 25 °C.

The switching of the $^1O_2$ photosensitizing ability of **B-2-S** upon addition of Cys is different from that of **B-1-S** (Fig. 14a). It was found that the $^1O_2$ photosensitizing ability of **B-2-S** increased in the presence of Cys (Φ_Δ = 71.5%) as compared with that in the absence of Cys (Φ_Δ = 16.7%). This is due to the recovered ISC of the PDT module after removal of the FRET by cleavage of the singlet energy acceptor,[39] and it is similar to that observed in the photodynamic molecular beacon.[14-16] If the excitation is into the

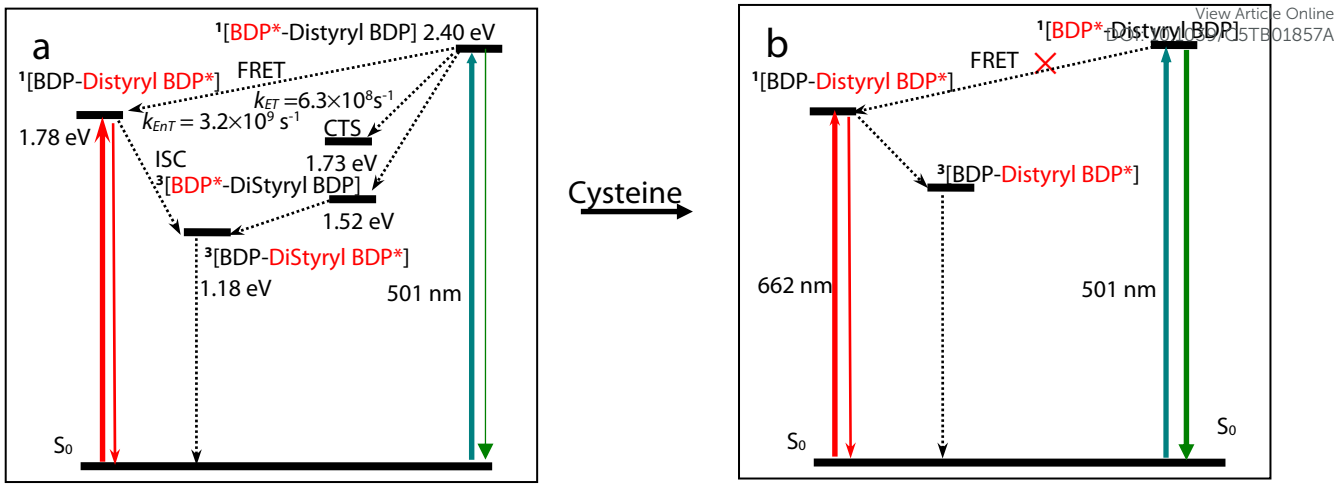

Scheme 3. Simplified Jablonski Diagram Illustrating the Photophysical Processes Involved in B-1-S (a) in the Absence of Cysteine and (b) in the Presence of Cysteine. [BDP-Distyryl BDP] stands for **B-1-S**. The component at the excited state was designated with red colour and a asterisk. The number of the superscript designated either the spin manifold. The fluorescence and the triplet state of **B-1-S** were switched by the presence and the absence of Cysteine. Note in the absence of Cysteine, the fluorescence of **B-1-S** were efficiently quenched by FRET. In the presence of Cysteine, disulfide bond is cleaved and FRET disappear, as a result the strong fluorescence of Bodipy were observed.

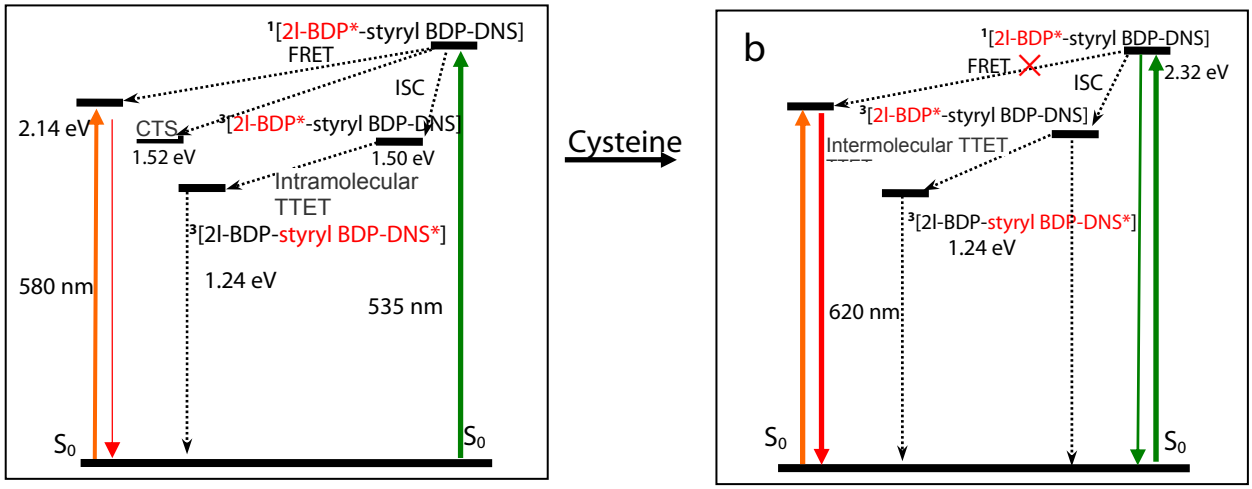

Scheme 4. Simplified Jablonski Diagram Illustrating the Photophysical Processes Involved in (a) **B-2-S** in the Absence of Cysteine and (b) **B-2-S** in the Presence of Cysteine. [I-BDP-styryl BDP-DNS] stands for **B-2-S**. The component at the excited state was designated with red colour and a asterisk. The number of the superscript designated the spin manifold. The fluorescence and the triplet state of **B-2-S** were switched by the presence and the absence of Cysteine. Note in the absence of Cysteine, the fluorescence of **B-2-S** were efficiently quenched by 2,4-nitrobenzenesulfonyl group. In the presence of Cysteine, both the disulfide bond and 2,4-nitrobenzenesulfonyl group are cleaved and RET disappears, as a result the strong fluorescence of Bodipy and high $^1O_2$ quantum yield were observed.

caged fluorescence module, negligible $^1O_2$ photosensitizing was observed due to the weak ISC of this module. It is noted that the sum of the fluorescence quantum yield and the $^1O_2$ yield is larger than 100%. Mono-chromophore based PDT/fluorescence bioimaging materials can only give the sum smaller than 100%.[19a]

For **B-2-C**, the $^1O_2$ photosensitizing ability is weak and was not affected by the addition of Cys (Fig. 14e). This result indicated that the ISC module in **B-2-C** was efficiently quenched by FRET, the charge recombination (CR) is inefficient to produce the triplet state, and the S−S linker is unable to be cleaved by Cys. Enhanced $^1O_2$ photosensitizing was observed for **B-3-S** in the presence of Cys, as compared to that of **B-3-S** alone (Fig. S80). This result indicated in **B-3-S**, the ISC of the PDT module is slightly quenched by the intramolecular charge transfer, which is supported by the calculation of the free energy changes of intramolecular electron transfer, and the low-lying CTS (at 1.0 eV). For **B-3-C**, however, the singlet oxygen photosensitizing is not affected by Cys. Recently Bodipy based dyad was studied with the fluorescence be switched ON in the presence of thiols, but the $^1O_2$ photosensitizing ability was not switched.[19b]

Switching ON of fluorescence and $^1O_2$ photosensitizing ability was observed with DNBS caged zinc(II) phthalocyanine photosensitizer, but the fluorescence and the $^1O_2$ photosensitizing

were accomplished with the same chromophore, thus the fluorescence and the $^1O_2$ photosensitizing cannot be maximized as **B-1-S** does.[19a]

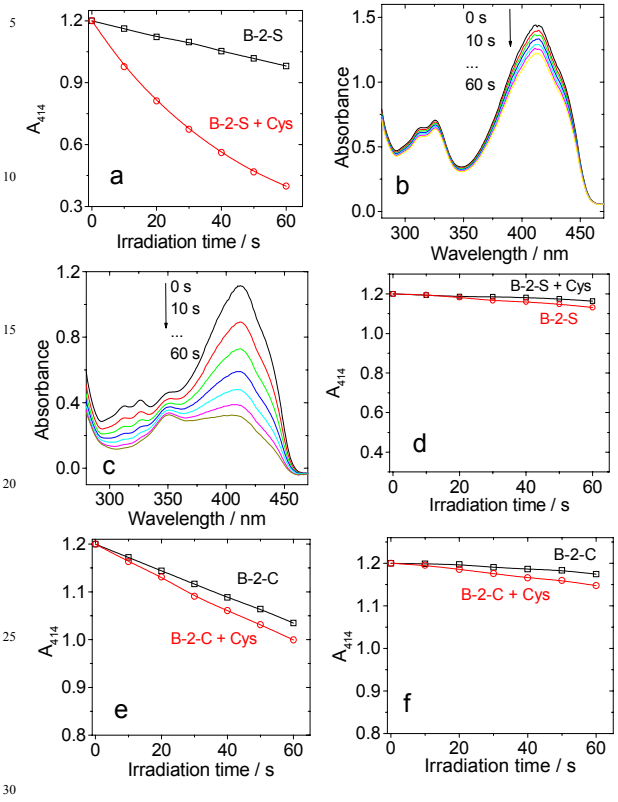

Fig. 14 Switching of the singlet oxygen ($^1O_2$) photosensitizing ability of the dyad **B-2-S** by Cys. The decreasing of the absorption of $^1O_2$ scavenger 1,3-diphenylisobenzofuran (DPBF) at 414 nm was monitored upon monochromic light irradiation. (a) Absorbance of DPBF at 414 nm changes in the absence and in the presence of Cys (λ_{ex} =535 nm) with **B-2-S** as photosensitizer. (b) UV–vis absorption spectral changes in the absence of Cys and (c) in the presence of Cys. (d) Absorption changes at 414 nm upon excitation at λ_{ex} = 586 nm. Change of the absorbance of DPBF at 414 nm in the absence and presence of Cys with **B-2-C** as triplet photosensitizer upon excitation at (e) 535 nm and (f) 586 nm. *c* [photosensitizers] = 1.0 × 10^{-5} M, *c*[Cys] = 3.0 × 10^{-3} M, in H_2O/DMF (v/v =1/4), pH = 7.4, 25 °C.

Intracellular luminescence Imaging and PDT Studies

The thiol-activatable fluorescence and PDT effect with the dyads were studied with HeLa cells.[23,61,62] After incubation of the HeLa cells with **B-1-S** for 3 h, intense green fluorescence was observed (Fig. 15e). With removal of the intracellular thiols by *N*-methylmaleimide, no such green fluorescence can be observed (Fig. 15e). These results demonstrated that the dyad **B-1-S** is selective to the intracellular thiols. Similar studies were carried out for **B-1-C**. No green fluorescence was observed after incubation with HeLa cells (See See ESI †, Fig. S81). This result indicates that the fluorescence was completely caged by the FRET effect.[42,63–65] We noted the abnormal morphology of the cell after incubation with **B-1-S**, but the reason for this change is unclear.

B-2-S was used for in situ detection of thiols in HeLa cell. Incubation of **B-2-S** in HeLa cells for 3 h, red fluorescence was observed (Fig. 16f). In order to further illustrate the red fluorescence come from the result in thiols and **B-2-S** reacted in the cell, *N*-methylmaleimide was used as the thiol scavenger. A control experiment was performed where the cellular thiols were removed using *N*-methylmaleimide before incubation of the cells with **B-2-S**. As a result, the red fluorescence was not observed (Fig. 16j). It shows that **B-2-S** can specifically detect thiols within the cell.

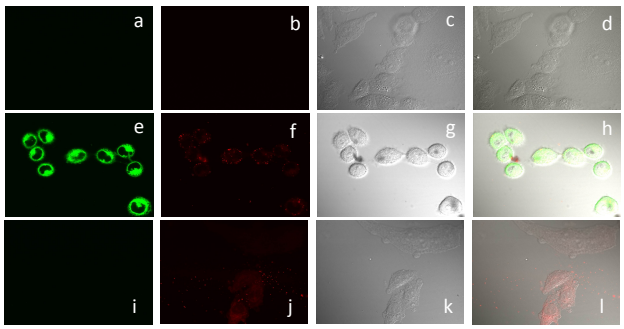

Fig. 15 Confocal laser scanning fluorescence microscopic images of HeLa cells. Luminescence images of HeLa cells without **B-1-S** at different excitation and imaging wavelength of (a) λ_{ex} = 488 nm, λ_{em} = 490–550 nm, and (b) λ_{ex} = 635 nm, λ_{em} = 650–750 nm. Luminescence images of HeLa cells incubated with **B-1-S** (25 μM) for 3 h, at different excitation and imaging wavelength of (e) λ_{ex} = 488 nm, λ_{em} = 490–550 nm, and (f) λ_{ex} = 635 nm, λ_{em} = 650–750 nm. Luminescence images of HeLa cells pretreated with *N*-methylmaleimide (0.5 mM) for 12 h and incubated with **B-1-S** (25 μM) for 3 h at different excitation and imaging wavelength of (i) λ_{ex} = 488 nm, λ_{em} = 490–550 nm and (j) λ_{ex} = 635 nm, λ_{em} = 650–750 nm. The corresponding bright field images of (d, h, l) are the overlay of respective luminescence (a, e, j) and bright images (c, g, k). 25 °C.

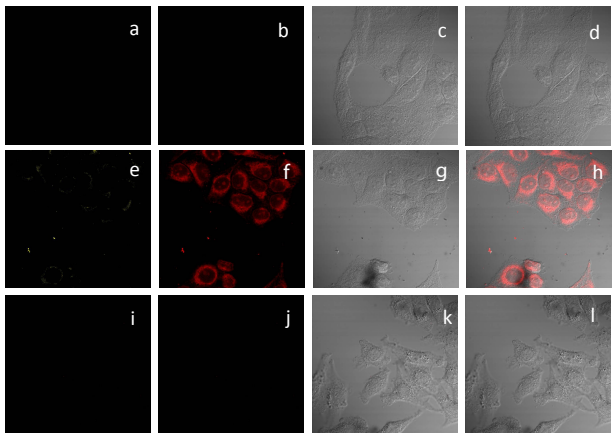

Fig. 16 Confocal laser scanning fluorescence microscopic images of HeLa cells. Luminescence images of HeLa cells upon excitation at different wavelength of (a) λ_{ex} = 488 nm, λ_{em} = 530–550 nm and (b) λ_{ex} = 559 nm, λ_{em} = 600 – 650 nm. Luminescence images of HeLa cells incubated with **B-2-S** (25 μM) for 3 h and then imaged at different excitation wavelength of (e) λ_{ex} = 488 nm, λ_{em} = 530–550 nm and (f) λ_{ex} = 559 nm, λ_{em} = 600–650 nm. Luminescence images of HeLa cells pretreated with *N*-methylmaleimide (0.5 mM) for 12 h and incubated with **B-2-S** (25 μM) for 3 h, and then imaged at different excitation wavelength of (i) λ_{ex} = 488 nm λ_{em} = 530–550 nm and (j) λ_{ex} = 559 nm, λ_{em} = 600–650 nm. 25 °C.

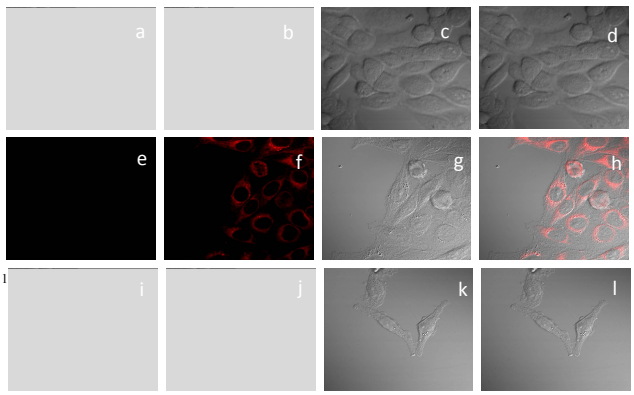

Fig. 17 Confocal laser scanning fluorescence microscopic images of HeLa cells. Luminescence images of HeLa cells upon excitation at different wavelength of (a) λ_{ex} = 488 nm, λ_{em} = 530–550 nm and (b) λ_{ex} = 559 nm, λ_{em} = 600 – 650 nm. Luminescence images of HeLa cells incubated with **B-2-C** (25 μM) for 3 h, upon different excitation wavelength at (e) λ_{ex} = 488 nm, λ_{em} = 530 – 550 nm and (f) λ_{ex} = 559 nm, λ_{em} = 600 – 650 nm. Luminescence images of cells pretreated with *N*-methylmaleimide (0.5 mM) for 12 h and incubated with **B-2-C** (25μM) for 3 h, upon different excitation wavelength at (i) λ_{ex} = 488 nm, λ_{em} = 530 – 550 nm and (j) λ_{ex} = 559 nm, λ_{em} = 600 – 650 nm. (c, g, k) are the corresponding bright field images of (a, e, i); (d, h, l) are the overlay of respective luminescence and bright images. 25 °C.

Later study shows that the PDT effect is significant, indicate that the linker between the PDT module and the fluorescence module was cleaved. After removal of the intracellular thiols by *N*-methylmaleimide, no red fluorescence can be observed.

Similar studies were carried out for **B-2-C**. Red fluorescence was observed after incubation with HeLa cells (Fig. 17f). After pre-treatment of the cells with *N*-methylmaleimide, no red fluorescence can be observed (Fig. 17j). However, our later study show that although the fluorescence can be un-caged by the intracellular thiols, the PDT ability of **B-2-C** cannot be activated by intracellular thiols

View Article Online
DOI: 10.1039/C5TB01857A

The cellular PDT effect with **B-2-S** and **B-2-C** as triplet photosensitizers was studied with an intracellular $^1O_2$ probe, DCFH-DA (Fig. 18).[48] Green fluorescence was observed for **B-2-S** with photoirradiation (Fig. 18g), but no such green emission was observed with **B-2-C** as the photosensitizer (Fig. 18e). Thus we conclude that no $^1O_2$ can be produced with **B-2-C**, but $^1O_2$ can be produced with **B-2-S** upon photoexcitation. Study in solution also show that the production of $^1O_2$ with **B-2-C** is negligible (Fig. 14f).

Table 5. IC_{50} values of **B-2-S** and **B-2-C** (μM) [a]

B-2-S		**B-2-C**	
In dark	With irradiation	In dark	With irradiation
30.1 ± 1.8	4.9 ± 0.27	29.6 ± 1.3	9.7 ± 0.45

[a] IC_{50}, the concentration of the compound that inhibits the proliferation rate by 50% compared with untreated cells, HeLa cell lines. Irradiated by a 515 – 525 nm LED, power intensity is 5 W/m^2.

IC_{50} values of **B-2-S** and **B-2-C** was studied in the absence and in the presence of photoirradiation by MTT assay (Table 5). IC_{50} values of **B-2-S** and **B-2-C** were found to be 37.50 μM and 31.25 μM, respectively, for HeLa cell lines. Moreover, In the presence of photoirradiation, much higher toxicity was observed, with IC50 values of 4.78 μM and 11.40 μM for **B-2-S** and **B-2-C**,respectively. IC_{50} values for **B-2-S** is lower than **B-2-C** because of disulfide bond was activation by thiols, but the caged PDT for **B-2-C** was not fully activated. The PDT effect of other compounds in Scheme 1 were not studied.

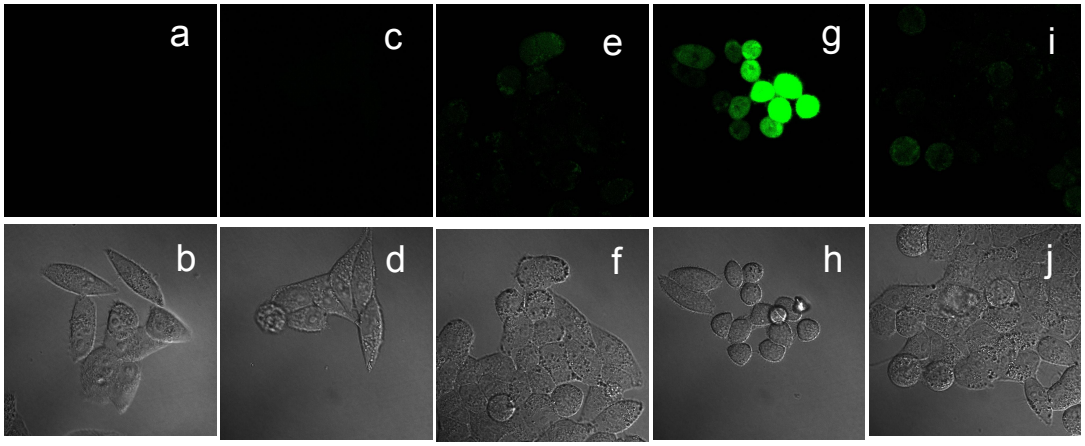

Fig. 18 Confocal laser scanning fluorescence microscopic images of the PDT effect on HeLa cells with **B-2-S** and **B-2-C** as the photosensitizers. **DCFH-DA** as intracellular singlet oxygen ($^1O_2$) probe. Imaging of cells without **B-2-S** and irradiation: (a) Dark field and (b) bright field images; Imaging of cells with **B-2-S** but without photoirradiation: (c) dark field and (d) bright field images; Imaging of cells with **B-2-C** and photoirradiation: (e) dark field and (f) bright field images; Imaging of cells with **B-2-S** and photoirradiation: (g) luminescence and (h) bright field images; Imaging of cells with **B-2-S** and photoirradiation, but pretreated with *N*-methylmaleicimide: (i) luminescence and (j) bright field images. *c* [photosensitizer] = 2.5 μM, *c*[**DCFH-DA**] = 2.0 μM, λ_{ex} = 488 nm, λ_{em} = 500 – 550 nm. For PDT study, the cells were incubated with the photosensitizers and the cells were irradiated by a 515 – 525 nm LED, power intensity is 5 W/m^2. 25 °C.

Conclusions

In conclusion, thiol-activatable bifunctional treatment/monitoring materials, i.e. photodynamic/fluorescence bioimaging dyads were prepared. The unique molecular structural profile of these dyads is that the activatable PDT and fluorescence were accomplished with two different chromophores (modules) in the dyad. Therefore, both the PDT and the fluorescence bioimaging effect can be maximized and the sum of the singlet oxygen ($^1O_2$) quantum yield (Φ_Δ) and the fluorescence yield (Φ_F) can be up to 200%. On the contrary, the conventional PDT/fluorescence bioimaging compounds were based on a *singlet* chromophore profile, thus the maximal sum of the $^1O_2$ yield and the fluorescence is only 100% because the intersystem crossing (producing triplet state) and the fluorescence process of the same chromophore is competitive. Herein we prepared six Bodipy dyads which contain both the caged PDT module and the caged fluorescence module. The linkers between the two modules in three dyads are bisulfide bonds (-S−S-), which can be selectively cleaved by intracellular thiols such as GSH and Cys. Caging of the fluorescence and production of triplet state is attained by either FRET or by cleavable quencher (2,4-dinitrobenzenesulfuride, DNS). In the presence of biological thiols such as Cys, disulfide linker was cleaved, as well as the DNS moiety, thus the PDT module and the fluorescence module were activated simultaneously. As a result, $^1O_2$ was produced upon photoexcitation and fluorescence was greatly enhanced (Φ_Δ: 16.7%→71.5%; Φ_F: 1.3%→47.6%;). Compared with the caged PDT/luminescent reagents based on a single chromophore, more efficient PDT effect and at the same time brighter luminescence bioimaging were attained with the dyad photosensitizers reported herein. Three reference dyads with un-cleavable -C−C- linker were prepared for comparison. The photophysical properties of the dyads were studied with steady state UV−vis absorption/fluorescence spectroscopies, as well as nanosecond time-resolved transient difference absorption spectroscopy. These results will be useful for the development of photodynamic/luminescence bioimaging bifunctional targeted-PDT reagents and the switching of the triplet state of organic compounds.

Acknowledgement

We thank the NSFC (21073028, 21273028, 21473020 and 21421005), the Royal Society (UK) and NSFC (China-UK Cost-Share Science Networks, 21011130154), Ministry of Education (SRFDP-20120041130005), the Fundamental Research Funds for the Central Universities (DUT14ZD226), Program for Changjiang Scholars and Innovative Research Team in University [IRT_132206] and Dalian University of Technology for financial support (DUT2013TB07).

Notes

[a] *State Key Laboratory of Fine Chemicals, School of Chemical Engineering, Dalian University of Technology, E-208 West Campus, 2 Ling Gong Rd., Dalian 116024, P. R. China. E-mail: zhaojzh@dlut.edu.cn Web: http://finechem2.dlut.edu.cn/photochem;*

[b] *School of Life Science and Biotechnology, Dalian University of Technology, Dalian 116024, P. R. China. E-mail: wuhj@dlut.edu.cn*

View Article Online
DOI: 10.1039/C5TB01857A

† Electronic Supplementary Information (ESI) available: molecular structure characterization data, UV-vis absorption spectra, fluorescence spectra and nanosecond transient absorption spectra. See DOI: 10.1039/b000000x

References

1 L. G. Arnaut, M. M. Pereira, J. M. Dąbrowski, E. F. F. Silva, F. A. Schaberle, A. R. Abreu, L. B. Rocha, M. M. Barsan, K. Urbańska, G. Stochel and C. M. A. Brett, *Chem. Eur. J.,* 2014, **20**, 5346– 5357.
2 F. Hu, F. Huang, G. Zhang, R. Zhao, H. Yang and D. Zhang, *Anal. Chem.,* 2014, **86**, 7987−7995.
3 A. Kamkaew, S. H. Lim, H. B. Lee, L. V. Kiew, L. Y. Chung and K. Burgess, *Chem. Soc. Rev*., 2013, **42**, 77−88.
4 J. Zhao, W. Wu, J. Sun and S. Guo, *Chem. Soc. Rev*., 2013, **42**, 5323−5351.
5 Y. Ichikawa, M. Kamiya, F. Obata, M. Miura, T. Terai, T. Komatsu, T. Ueno, K. Hanaoka, T. Nagano and T. Urano, *Angew. Chem. Int. Ed*., 2014, **53**, 6772–6775.
6 F. Doria, I. Manet, V. Grande, S. Monti and M. Freccero, *J. Org. Chem.,* 2013, **78**, 8065−8073.
7 A. Gorman, J. Killoran, C. O'Shea, T. Kenna, W. M. Gallagher and D. F. O'Shea, *J. Am. Chem. Soc.,* 2004, **126**, 10619−10631.
8 T. Yogo, Y. Urano, Y. Ishitsuka, F. Maniwa and T. Nagano, *J. Am. Chem. Soc.,* 2005, **127**, 12162−12163.
9 S. H. Lim, C. Thivierge, P. Nowak-Sliwinska, J. Han, H. van den Bergh, G. Wagnières, K. Burgess and H. B. Lee, *J. Med. Chem.,* 2010, **53**, 2865–2874.
10 M-R. Ke, S-R. Yeung, D. K. P. Ng, W-P. Fong and P-C. Lo, *J. Med. Chem.,* 2013, **56**, 8475−8483.
11 T. Lu, P. Shao, I. Mathew, A. Sand and W. Sun, *J. Am. Chem. Soc.,* 2008, **130**, 15782–15783.
12 J. F. Lovell, M. W. Chan, Q. Qi, J. Chen and G. Zheng, *J. Am. Chem. Soc.,* 2011, **133**, 18580–18582.
13 X-J. Jiang, S-L. Yeung, P-C. Lo, W-P. Fong and D. K. P. Ng, *J. Med. Chem.,* 2011, **54**, 320–330.
14 G. Zheng, J. Chen, K. Stefflova, M. Jarvi, H. Li and B. C. Wilson, *Proc. Natl. Acad. Sci. U.S.A.,* 2007, **104**, 8989–8994.
15 A. M. Bugaj, *Photochem. Photobiol. Sci.,* 2011, **10**, 1097–1109.
16 P-C. Lo, J. Chen, K. Stefflova, M. S. Warren, R. Navab, B. Bandarchi, S. Mullins, M. Tsao, J. D. Cheng and G. Zheng, *J. Med. Chem.,* 2009, **52**, 358–368.
17 L. Hou, X. Zhang, T. C. Pijper, W. R. Browne and B. L. Feringa, *J. Am. Chem. Soc.,* 2014, **136**, 910−913.
18 S. Erbas-Cakmak and E. U. Akkaya, *Angew. Chem. Int. Ed.,* 2013, **52**, 11364–11368.
19 (a) H. He, P-C. Lo and D. K. P. Ng, *Chem. Eur. J.,* 2014, **20**, 6241–6245. (b) S. Erbas-Cakmak and E. U. Akkaya, *Org. Lett.,* 2014, **16**, 2946−2949.
20 Z. Tang, Z. Zhu, P. Mallikaratchy, R. Yang, K. Sefah and W. Tan, *Chem. Asian J.,* 2010, **5**, 783 – 786.
21 (a) M. H. Lee, Z. Yang, C. W. Lim, Y. H. Lee, S. Dongbang, C. Kang and J. S. Kim, *Chem. Rev.,* 2013, **113**, 5071−5109. (b) Z. Yang, J. H. Lee, H. M. Jeon, J. H. Han, N. Park, Y. He, H. Lee, K. S. Hong, C. Kang and J. S. Kim, *J. Am. Chem. Soc.,* 2013, **135**, 11657−11662.
22 X. Wu, X. Sun, Z. Guo, J. Tang, Y. Shen, T. D. James, H. Tian and W. Zhu, *J. Am. Chem. Soc.,* 2014, **136**, 3579−3588.
23 L. Zhang, D. Duan, Y. Liu, C. Ge, X. Cui, J. Sun and J. Fang, *J. Am. Chem. Soc.,* 2014, **136**, 226−233.
24 (a) X. Chen, Y. Zhou, X. Peng and J. Yoon, *Chem. Soc. Rev.,* 2010, **39**, 2120–2135. (b) S. Santra, C. Kaittanis, O. J. Santiesteban and J. M. Perez, *J. Am. Chem. Soc.,* 2011, **133**, 16680–16688.
25 Y. Cho and Y. Choi, *Chem. Commun.,* 2012, **48**, 9912–9914.
26 H. Kim, S. Mun and Y. Choi, *J. Mater. Chem. B.,* 2013, **1**, 429–431.
27 J. T. F. Lau, P-C. Lo, X-J. Jiang, Q. Wang and D. K. P. Ng, *J. Med. Chem.,* 2014, **57**, 4088−4097.

28 W. Jiang, Q. Fu, H. Fan, J. Ho and W. Wang, *Angew. Chem. Int. Ed.,* 2007, **46**, 8445–8448.

29 J. Bouffard, Y. Kim, T. M. Swager, R. Weissleder and S. A. Hilderbrand, *Org. Lett.,* 2008, **10**, 37–40.

30 Y. Chen, J. Zhao, H. Guo and L. Xie, *J. Org. Chem.,* 2012, **77**, 2192−2206.

31 H. Guo, Y. Jing, X. Yuan, S. Ji, J. Zhao, X. Li and Y. Kan, *Org. Biomol. Chem.,* 2011, **9**, 3844–3853.

32 J. Shao, H. Sun, H. Guo, S. Ji, J. Zhao, W. Wu, X. Yuan, C. Zhang and T. D. James, *Chem. Sci.,* 2012, **3**, 1049–1061.

33 S. Ji, H. Guo, X. Yuan, X. Li, H. Ding, P. Gao, C. Zhao, W. Wu, W. Wu and J. Zhao, *Org. Lett.,* 2010, **12**, 2876–2879.

34 A. Loudet and K. Burgess, *Chem. Rev.,* 2007, **107**, 4891−4932.

35 G. Ulrich, R. Ziessel and A. Harriman, *Angew. Chem. Int. Ed.,* 2008, **47**, 1184–1201.

36 R. Ziessel and A. Harriman, *Chem. Commun.,* 2011, **47**, 611–631.

37 H. Lu, J. Mack, Y. Yang and Z. Shen, *Chem. Soc. Rev.,* 2014, **43**, 4778–4823.

38 Y. Cakmak, S. Kolemen, S. Duman, Y. Dede, Y. Dolen, B. Kilic, Z. Kostereli, L. T. Yildirim, A. L. Dogan, D. Guc and E. U. Akkaya, *Angew. Chem. Int. Ed.,* 2011, **50**, 11937–11941.

39 S. Erbas-Cakmak, O. A. Bozdemir, Y. Cakmak and E. U. Akkaya, *Chem. Sci.,* 2013, **4**, 858–862.

40 M. Baruah, W. Qin, C. Flors, J. Hofkens, R. A. L. Vallée, D. Beljonne, M. V. der Auweraer, W. M. D. Borggraeve and N. Boens, *J. Phys. Chem. A.,* 2006, **110**, 5998–6009.

41. M. T. Whited, P. I. Djurovich, S. T. Roberts, A. C. Durrell, C. W. Schlenker, S. E. Bradforth and M. E. Thompson, *J. Am. Chem. Soc.,* 2011, **133**, 88–96.

42 M. E. El-Khouly, A. N. Amin, M. E. Zandler, S. Fukuzumi and F. D′Souza, *Chem. Eur. J.,* 2012, **18**, 5239–5247.

43 S. Ji, J. Yang, Q. Yang, S. Liu, M. Chen and J. Zhao, *J. Org. Chem.,* 2009, **74**, 4855–4865.

44 L. Yi, H. Li, L. Sun, L. Liu, C. Zhang and Z. Xi, *Angew. Chem. Int. Ed.,* 2009, **48**, 4034–4037.

45 Z. Kostereli, T. Ozdemir, O. Buyukcakir and E. U. Akkaya, *Org. lett.,* 2012, **14**, 3636–3639.

46 A. Harriman, M. A. H. Alamiry, J. P. Hagon, D. Hablot and R. Ziessel, *Angew. Chem. Int. Ed.,* 2013, **52**, 6611–6615.

47 B. Zhu, X. Zhang, Y. Li, P. Wang, H. Zhang and X. Zhuang, *Chem. Commun.,* 2010, **46**, 5710–5712.

48 J. Tian, L. Ding, H-J. Xu, Z. Shen, H. Ju, L. Jia, L. Bao and J-S. Yu, *J. Am. Chem. Soc.,* 2013, **135**, 18850−18858. DOI: 10.1039/C5TB01857A

49 W. Wu, J. Zhao, J. Sun and S. Guo, *J. Org. Chem.* 2012, **77**, 5305−5312.

50 T. Lazarides, T, M. McCormick, K. C. Wilson, S. Lee, D. W. McCamant and R. Eisenberg, *J. Am. Chem. Soc.,* 2011, **133**, 350–364.

51 K. Feng, M-L.Yu, S-M. Wang, G-X. Wang, C-H. Tung and L-Z. Wu, *ChemPhysChem.,* 2013, **14**, 198–203.

52 M. E. El-Khouly and S. Fukuzumi, *J. Porphyrins Phthalocyanines.,* 2011, **15**, 111–117.

53 J. Ma, X. Yuan, B. Küçüköz, S. Li, C. Zhang, P. Majumdar, A. Karatay, X. Li, H. G. Yaglioglu, A. Elmali, J. Zhao and M. Hayvali, *J. Mater. Chem. C.,* 2014, **2**, 3900–3913.

54 S. Guo, L. Ma, J. Zhao, B. Küçüköz, A. Karatay, M. Hayvali, H. G. Yaglioglu and A. Elmali, *Chem. Sci.,* 2014, **5**, 489–500.

55 L. Huang, X. Cui, B. Therrien and J. Zhao, *Chem. Eur. J.,* 2013, **19**, 17472– 7482.

56 P. A. van Hal, J. Knol, B. M. W. Langeveld-Voss, S. C. J. Meskers, J. C. Hummelen and R. A. J. Janssen, *J. Phys. Chem. A.,* 2000, **104**, 5974–5988.

57 J. J. Apperloo, C. Martineau, P. A. van Hal, J. Roncali and R. A. J. Janssen, *J. Phys. Chem. A.,* 2002, **106**, 21−31.

58 R. Ziessel, B. D. Allen, D. B. Rewinska and A. Harriman, *Chem. Eur. J.,* 2009, **15**, 7382–7393.

59 J-Y. Liu, M. E. EI-Khouly, S. Fukuzumi and F. D′Souza, *Chem. Asian J.,* 2011, **6**, 174–179.

60 S-H. Lee, C. T-L. Chan, K. M-C. Wong, W. H. Lam, W-M. Kwok and V. W-W. Yam, *J. Am. Chem. Soc.,* 2014, **136**, 10041−10052.

61 J. H. Lee, C. S. Lim, Y. S. Tian, J. H. Han and B. R. Cho, *J. Am. Chem. Soc*., 2010, **132**, 1216–1217.

62 B. K. McMahon and T. Gunnlaugsson, *J. Am. Chem. Soc.,* 2012, **134**, 10725−10728.

63 X. Zhang, Y. Xiao and X. Qian, *Org. Lett.,* 2008, **10**, 29–32.

64 O. A. Bozdemir, S. Erbas-Cakmak, O. O. Ekiz, A. Dana and E. U. Akkaya, *Angew. Chem. Int. Ed.,* 2011, **50**, 10907–10912.

65 J. Fan, M. Hu, P. Zhan and X. Peng, *Chem. Soc. Rev.,* 2013, **42**, 29–43.

View Article Online
DOI: 10.1039/C5TB01857A

Graphical Abstract:

Maximizing the Thiol-Activated Photodynamic and Fluorescence Imaging Functionalities of Theranostic Reagents by Modularization: Preparation and Study of the Switching of Triplet Excited State

By *Jianzhang Zhao,[a,]* Ling Huang,[a] Xiaoneng Cui,[a] Shujing Li,[b] and Huijian Wu[b,]**

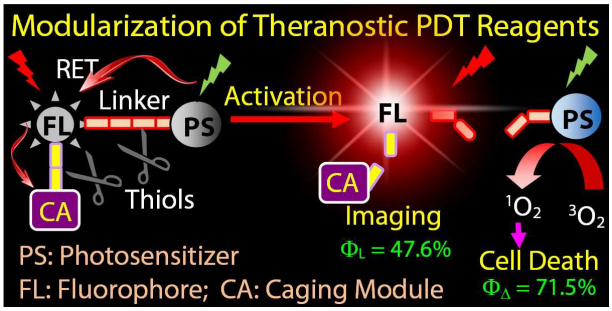

The fluorescence imaging and the singlet oxygen production ability of the thiol-cleavable triplet photosensitizers was maxized by disintergration the functionalities.